Analysis of Tissue Sparing and Circuit Regeneration in Spinal Cord Injuries Treated with Biomaterials and Gene Therapy

by

Jessica Chen

A dissertation submitted in partial fulfillment
of the requirements for the degree of
Doctor of Philosophy
(Neuroscience)
in the University of Michigan
2020

Doctoral Committee:

Professor Lonnie Shea, Chair
Associate Professor Catherine Collins
Professor Eva Feldman
Assistant Professor Daniel Leventhal
Associate Professor Bing Ye

Jessica Chen

chenjess@umich.edu

ORCID ID: 0000-0002-4833-6756

Table of Contents

List of Tables

List of Figures

Abstract

Each year, the U.S. sees nearly 17,700 new cases of spinal cord injuries (SCIs) [1]. Despite intense rehabilitation, patients with SCIs most often suffer lifelong physical consequences and substantial increases in medical expenses per individual [2]. While immobilization and surgery can be used for immediate stabilization of the injury, no clinical methods exist to address the subsequent inflammation and lack of tissue regeneration that further contribute to the motor and sensory deficits seen after an SCI [3, 4]. This dissertation aimed to understand how biomaterials and gene therapy treatment affect SCIs.

In a mouse SCI model, where a left C5 hemisection results in loss of function of the left arm, a poly(lactide-co-glycolide) (PLG) scaffold or "bridge" can be implanted in place of the resected tissues. The bridge can be loaded with lentivirus for local delivery of gene therapy that can aid in control of the post-SCI microenvironment [5]. Using lentiviral interleukin-10 (IL10), we found that IL10 animals significantly outperform animals that received a control lentivirus on a ladder beam test at 2- and 12- weeks post-injury (wpi). Closer examination of components of the forelimb motor circuitry suggest IL10 animals had increased sparing of lower motor neurons and neuromuscular junctions. Electrophysiological studies at 2 wpi showed that control injured animals had electromyogram recordings that were significantly dampened when compared to IL10 and control uninjured animals, thereby confirming that the motor circuitry remained more intact with IL10 treatment. These results, which were consistent in both male and female mice,

are the first to show that IL10 spares motor circuitry directly responsible for enhanced muscle function.

We then tested a combination therapy of lentiviral IL10 and brain-derived neurotrophic factor (BDNF), followed by examination of tissue sparing and regeneration. At 2 wpi, histological and electrophysiological analyses show that the tissue sparing effects of IL10 alone are only slightly enhanced by the addition of BDNF. By 12 wpi, most innervation differences among the treatment conditions disappeared, though electrophysiological examination suggests that IL10 may prevent some of the injury-associated shifts in muscle composition that result in increased fatigability in control injured animals. Within the spinal cord, we found that IL10 alone and IL10+BDNF cause a similar increase in axon growth across the injury site. 3D imaging using Clear Lipid-exchanged Acrylamide-hybridized Rigid Imaging / Immunostaining / in situ-hybridization-compatible Tissue Hydrogel (CLARITY) shows these axons do completely traverse the injury site, while electrophysiological studies suggest these axons are able to carry action potentials. These results are the first to show that regenerated axons can be electrophysiologically active.

Taken together, these studies suggest early immunomodulation can have long-lasting benefits through tissue sparing, and that regenerated axons have the potential to transduce signals across an injury site. These findings provide novel insights into how the pathophysiology following an SCI can be altered using biomaterials and gene therapy. Future studies will involve identifying the synaptic targets of regenerated axons and determining how the formation of new circuits can influence motor function.

Chapter 1 Introduction

Opening

After an SCI, the loss of specific neural connections and inadequate regeneration of motor circuitry often results in life-long paralysis. The research in this dissertation aims to better understand the pathophysiology following an injury and how anti-inflammatory or neurotrophic gene therapy can influence recovery. This work identifies motor circuit components that can be spared from secondary damage and examines the anatomical and electrophysiological properties of regenerated axons.

Thesis Overview

Chapter 1 introduces the major research outcomes presented in this dissertation.

Chapter 2 outlines existing research that is pertinent to understanding the advances made by this dissertation.

Chapter 3 investigates muscle innervation and tissue sparing immediately following acute bridge implantation with and without anti-inflammatory IL10 gene therapy. These studies identify components of the motor circuitry that are spared from secondary damage and investigate their electrophysiological properties in both male and female mice. This chapter demonstrates that IL10's therapeutic benefits act through the sparing of circuits involved in motor control, thereby providing a neuroanatomical explanation behind the efficacy of IL10 as a pre-clinical treatment for modulating post-SCI inflammation.

Chapter 4 investigates muscle atrophy and axon regeneration seen after acute bridge implantation in response to treatment with IL10 and/or BDNF. These studies aim to identify changes in muscle composition and fatigability that can affect motor function and investigate the electrophysiological properties of regenerating axons. Preliminary results suggest that some of the increased muscle fatigability seen after an SCI can be prevented using IL10 treatment. Furthermore, this chapter demonstrates that regenerated axons can carry electrical signals across the injury site. Ongoing histological studies aim to reveal how post-SCI muscle fiber type shifts are affected by gene therapy treatment. Finally, exponential modeling of electromyogram recordings is used to quantify signal decay rates to better understand how muscle activation and fatigue are affected by an SCI, fiber type shifting, and therapeutic treatment.

Chapter 5 summarizes the results presented, recommends routes for future directions, and concludes the dissertation.

Chapter 2 Overview of Spinal Cord Repair

Significance

The World Health Organization estimates that up to 500,000 people each year will sustain a spinal cord injury (SCI) [6]. Cervical injuries are both the most prevalent, making up between 49.3-61.5% of all SCIs [7], and the most detrimental since loss of function can be seen in nearly all systems innervated at and caudal to the injury level. Risk per individual peaks during adolescence in women and young adulthood in men, and again later in life [6]. These injuries almost always result in chronic pain, and permanent sensory and motor deficits. For those who survive an SCI, the long-term consequences include a myriad of life-long and devastating financial, social, and physical limitations [8].

Neuroinflammation and Secondary Damage

SCIs can be classified as traumatic or non-traumatic. Non-traumatic injuries can be caused by diseases, infections, tumors, or stroke [9]. Traumatic injuries can be further classified into penetrating or non-penetrating. Non-penetrating injuries include contusions, compressions, or stretch injuries, whereas penetrating injuries are most often caused by motor vehicle or sporting accidents [1]. Within 15 minutes following any type of SCI, there is an upregulation of a multitude of inflammatory cytokines and chemokines from microglia, the resident macrophages of the central nervous system [10]. Additionally, breakage of the blood-brain barrier allows for the infiltration of neutrophils that help amplify the injury response by releasing proteases that disrupt the extracellular matrix and allow for increased infiltration of peripheral monocytes [10-

13]. In response to the microenvironment, these peripheral monocytes will then differentiate into macrophages that can take on one of two phenotypes. The pro-inflammatory phenotype is designed to kill invading pathogens and virus-infected cells [14]. This cascade of feed-forward events represents the innate immune response, which is hypothesized to be designed by evolution to protect humans from infection. However, in the context of an SCI, molecules that are associated with this phenotype can cause increased demyelination and neuronal apoptosis, thereby exacerbating the primary injury [3, 15, 16]. Meanwhile, the anti-inflammatory phenotype encourages cell survival and tissue regeneration through the production of growth factors [14]. Thus, preventing the post-injury inflammation that results in secondary damage is a clear target for therapeutic intervention.

Strategies for Controlling Inflammation

Several studies have shown that early anti-inflammatory treatment has neuroprotective benefits [17]. Methylprednisolone is the only general immunosuppressant that has been widely used as the standard of care for acute SCIs. However, more recent studies have shown that its therapeutic benefits are marginal to none, while its adverse side effects are dangerous [18-21]. Furthermore, general immunosuppression is unsuitable after an SCI, because it increases infection rates and decreases pro-regenerative immune cell functions [22]. Alternatively, cellular and molecular approaches for reducing inflammation are more promising because they offer increased specificity. Studies have shown that neutrophil and macrophage depletion or neutralization can improve recovery after an SCI [23, 24], while transplantation of certain macrophages and microglia can promote regeneration following the injury [25-27]. The outcome is heavily dependent on the phenotype of these inflammatory cells, which depends on the ligands that activate them [22, 28]. For example, IL10 is a cytokine that is both expressed by

macrophages [29], and used for polarizing macrophages towards the anti-inflammatory phenotype [30]. IL10 downregulates pro-apoptotic factors and upregulates anti-apoptotic factors, as well as provides trophic support to neurons through the IL10 receptor [31, 32]. In the absence of IL10, secondary damage is exacerbated [29, 33].

The Shea Lab has been actively exploring the profound neuroprotective effects of lentivirus-mediated delivery of the IL10 gene under a CMV promotor. Since inflammation and regeneration can take upwards of weeks, the ability to locally induce sustained gene expression provides an enormous advantage for long-term modulation of the injury microenvironment. The Shea Lab has shown that local gene delivery can result in transgene expression, by mainly Schwann cells, fibroblasts, and macrophages, that remains for weeks after implantation [5, 34]. Thus far, lentiviral IL10 has been shown to promote and sustain anti-inflammatory polarization of peri-injury immune cells [35], reduce post-injury inflammation [36], and enhance functional recovery [37].

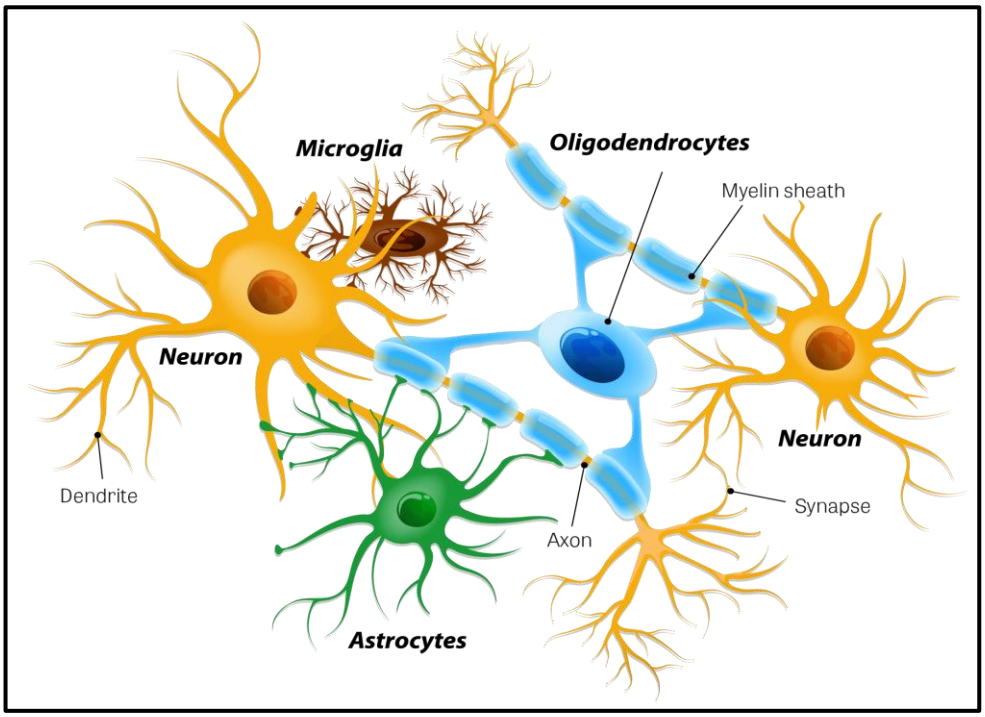

Figure 1. Cells of the Nervous System.

Spinal Cord Circuitry and Regeneration

The cell type that is mainly responsible for the transmission of information is the neuron (**Figure 1.** Cells of the Nervous System) [38]. Each neuron can have axons or dendrites, which are responsible for transmitting and receiving information, respectively. The location where one neuron contacts another neuron, via axons and dendrites, is a synapse, which is surrounded by astrocytes that help maintain the microenvironment and regulate neurotransmitter concentrations. Myelinating oligodendrocytes help facilitate the transduction of information along axons by providing insulation. Meanwhile, microglia migrate through tissues to survey for damages and pathogens.

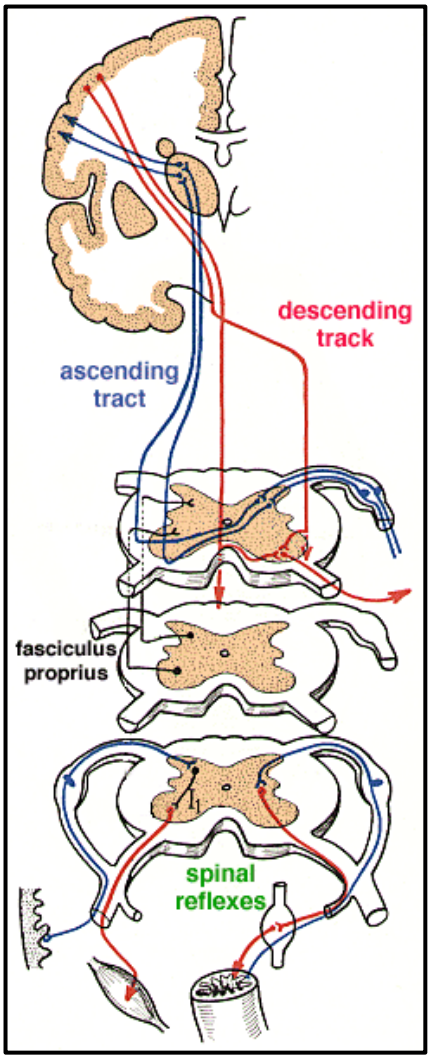

Figure 2. Tracts of the spinal cord.

Spinal circuits have three main directions of information transfer (**Figure 2**) [39]. First, ascending tracts are responsible for transmitting sensory information, such as touch, pain, temperature, or limb location. Neurons whose cell bodies reside in the dorsal root ganglia collect and send information from the periphery to the brain. Second, descending tracts are responsible for transmitting motor information, such as balance, posture, and fine motor control. Neurons whose cell bodies reside in the ventral gray matter of the spinal cord receive and send information from the brain to the periphery. Finally, spinal reflex tracts are responsible for immediate sensory to motor information processing, such as for the coordination of a reflex or maintenance of muscle tone. Neurons whose cell bodies reside in the dorsal root ganglia and throughout the gray matter within a spinal level can receive and send information from and to the periphery with or without cortical input.

In both mice and humans, the corticospinal tract (CST) is responsible for fine motor control of skeletal muscles. The CST is composed of upper motor neurons (UMNs), whose cell bodies are located in layer V of the motor cortex and whose axons travel down the spinal cord to synapse directly or indirectly, via an interneuron, onto lower motor neurons (LMNs). In rodents, the direct UMN-LMN connection only exists for the first two postnatal weeks [40-43]. The LMN, located in the ventral gray matter of the spinal cord, sends axons that exit the spinal cord, through the ventral root, and synapse onto skeletal muscles associated with the spinal cord level in which the LMN is located. Disruption of the UMN to LMN connection will prevent the transmission of voluntary motor information from the brain to the muscle, which is why paralysis so often results from an SCI [44]. After an injury, UMNs transiently express growth and regeneration genes such as growth-associated protein (GAP-43) that is found in growth cones [45-47]. However, in the absence of trophic factors and in the presence of growth

inhibitory factors, the intrinsic regenerative potential of injured neurons is not sustained [48]. Furthermore, scar formation results in a physical barrier that prevents axonal elongation across the injury site [49]. Therefore, while injured UMNs do hold the innate capacity for axon regeneration, these axons meet both physical and chemical barriers that prevent reestablishment of the UMN to LMN connection.

Strategies for Promoting Regeneration

While reducing inflammation will work to prevent further damage, the preceding mechanical insult will inevitably disrupt circuits that are critical for transmitting electrical information along the spinal cord. Some neurons, astrocytes, and oligodendrocytes will still undergo apoptosis, while severely damaged axons and synapses will degenerate. For behavioral recovery to continue beyond the inflammatory period, either the surviving circuits need to rewire to accommodate the loss or the damaged circuits need to regenerate to replace what is lost. Aside from stabilization and decompression, no clinical intervention currently exists for managing an SCI [50]. Once inflammation has subsided, and when macrophages are done clearing tissue debris, what remains of the lesion site is a fluid-filled cyst that is surrounded by scar tissues [51]. Studies have shown that filling the lesion site with a biomaterial can help prevent cyst formation [52]. Without a scar and cyst that act as mechanical barriers, and with a synthetic extracellular matrix (ECM) along which axons can grow, regeneration becomes more feasible. Both natural biomaterials that are normally found in the ECM of animal tissues (i.e. collagen, laminin, fibronectin) and synthetic biomaterials that have tunable porosities and degradation rates (i.e. poly(ethylene glycol), poly (2-hydroxyethyl methylacrylate), poly(lactide-co-glycolide)) have been explored for implantation into an SCI with varying extents of increased axon regeneration and motor recovery [34, 52-66].

As an alternative to changing the mechanical microenvironment using biomaterials, the chemical microenvironment may also be modified to support regeneration. For example, transplanted neural, embryonic, and induced pluripotent stem cells can release neurotropic factors, lay an ECM, and differentiate into neurons, oligodendrocytes, and astrocytes, resulting in improved motor recovery [67-78]. Specific proteins such as hepatocyte growth factor or fibroblast growth factor have shown limited success in improving SCI pathophysiology and subsequent motor function [79, 80]. However, localized delivery is difficult and protein half-life is too short for a single application. Thus, attention has shifted towards the use of viral vectors for localized, stable, and sustained gene expression. For example, adenoviruses, herpes simplex viruses, and lentiviruses have all been used to deliver neurotrophic factors to increase axon regeneration and improve behavioral outcomes [37, 81-85].

Changes to the mechanical and chemical microenvironments have been independently successful, thereby begging the question of whether a combinatorial therapy would further increase regeneration and recovery. BDNF is a secreted protein that, under developmental and homeostatic conditions, encourages growth and differentiation of new neurons and synapses. Studies have shown that delivery of BDNF, which also has anti-inflammatory effects [86], in combination with stem cells and/or biomaterials can result in positive histological and/or behavioral outcomes [87-103].

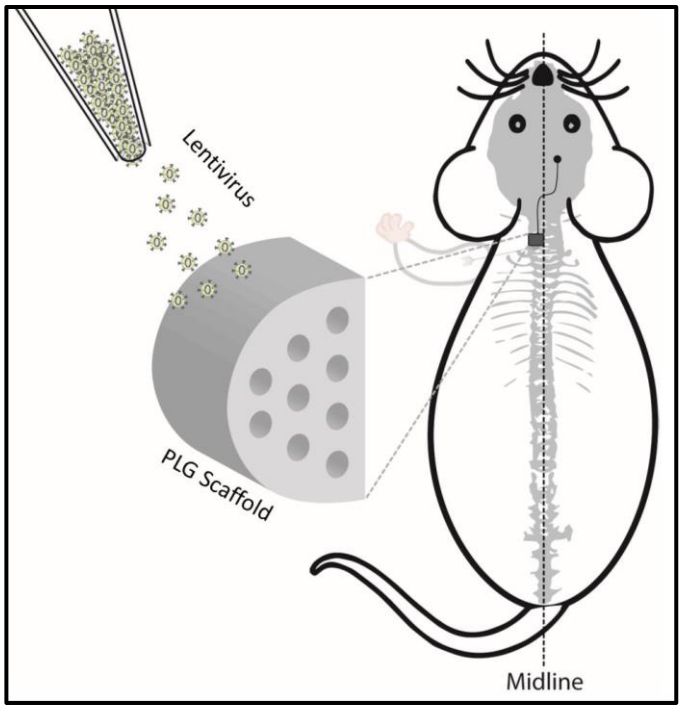

Figure 3. Biomaterial implant with lentiviral gene therapy.

The Shea lab has developed a scaffold implant made of poly(lactide-co-glycolide) (PLG) that is degradable via hydrolysis (**Figure 3**). Implantation of this biomaterial "bridge" that bridges the gap left by a lateral hemisection has many advantages. First, it clearly delineates between intact and regenerated tissues, since axons observed within the bridge are considered to be regenerated [104]. Second, the time course of degradation is tuned for seamless integration with host tissues during the wound healing process. Third, its porosity is optimized to allow for adequate cell infiltration and adherence. Finally, it contains 9 channels that traverse the anterior-posterior axis of the injury, thereby acting as a conduit that provides mechanical support for axon growth [50]. Bridge implantation results in the regeneration of CST axons into the injury site and re-entry of these axons into the spinal tissues caudal to the injury site [104]. The efficacy of the bridge may be further augmented through the use of lentiviral gene therapy [105]. The Shea lab has shown that lentiviral BDNF via a PLG scaffold can enhance axon growth and myelination after an SCI [34]. Thus far, lentiviral neurotrophin-3, interleukin-4, platelet-derived growth

factor, and noggin, and even spinal progenitor cells have all been delivered via the bridge with a multitude of favorable outcomes [34, 37, 69, 106].

Muscles After a Spinal Cord Injury

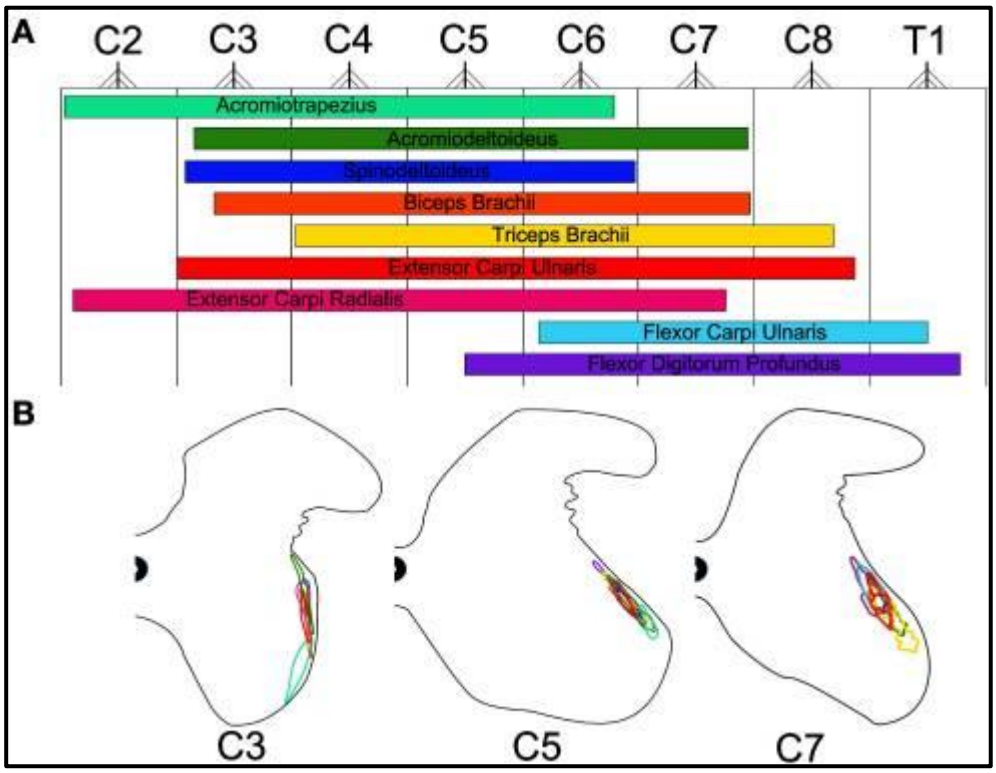

Figure 4. Muscles of the forelimb are innervated by different cervical levels.

The connection between an LMN and a muscle fiber is called a neuromuscular junction (NMJ), whereas each set of muscle fibers innervated by an LMN make up a motor unit [107]. Along the spinal cord, LMNs are topographically connected to different muscle groups. Since UMN axons descend caudally to their respective LMN targets, an SCI can sever cortical input to all spinal levels caudal to the injury. Therefore, both direct LMN loss and indirect reductions in LMN activation, due to decreased cortical input, can contribute to the paralysis of muscle groups represented at and caudal to the injury level (**Figure 4**) [108].

The axons of an inactive, damaged, or deceased LMN will degenerate, resulting in NMJ denervation of muscle fibers within that motor unit [109]. Denervated NMJs will then release

factors that drive re-innervation by the sprouting of nearby axons [110, 111], which is possible because LMNs express genes associated with growth and regeneration to a higher extent than UMN and because the peripheral nervous system has far fewer inhibitory cues for regeneration [46, 112]. If a denervated NMJ is captured by the sprouting of a nearby axon, that muscle fiber can now survive as an adoptee into another motor unit. However, if a denervated NMJ experiences a prolonged absence of neural input, the muscle fiber will atrophy and this atrophy is associated with a decrease in muscle contraction force [113-117]. In humans, muscle atrophy starts within a few days after an SCI, followed by fiber-type transformation [118-121].

A single muscle is composed of different fiber types that atrophy at different rates immediately post-injury, but to the same extent after prolonged disuse and denervation [122, 123]. Type I fibers, which atrophy at slower rates, generate low forces that can be sustained for long periods of time and are therefore considered to be slow-fatiguing or fatigue resistant. Type II fibers, which can generate high forces when activated, fatigue and atrophy more quickly than type I fibers [124-130]. Type II fibers are further classified as IIa, IIb, and IIx, which fall along a spectrum that can be defined by differences in characteristics such as contraction speed, fatigue resistance, oxidative metabolism, glycolytic metabolism, vascularization, and fiber diameter [131]. Different muscles are composed of different combinations of type I, IIa, IIb, and IIx fibers [132]. The effects that an SCI has on muscle composition can be due to either differences in fiber type atrophy rates or by “type-shifting” where a fiber can change to a different phenotype [130, 133-136]. After an SCI, dynamic shifts in motor units, muscle size, and fiber types means a loss of fine motor control, reduced strength, and decreased resistance to fatigue [109, 137, 138].

Strategies for Preventing Muscle Atrophy

To varying degrees, treadmill training, delivery of neurotrophic factors, stem cell transplantation, and electrical/magnetic stimulation after an SCI have been shown to independently or combinatorially promote muscle fiber formation, prevent atrophy, and enhance motor recovery [139-154]. In cases of incomplete SCIs, where some cortical input for voluntary movement remains intact, prevention of muscle atrophy can significantly contribute to rehabilitation outcomes [155]. However, the strategies employed to combat post-SCI muscular changes decrease in efficacy with increasing SCI severity. In cases of complete SCIs, where there is a permanent loss of cortical input for voluntary movement, muscle size and composition cannot be maintained without ongoing rehabilitation. Therefore, preservation or reestablishment of motor circuitry must necessarily coincide with the prevention of muscle atrophy in patients with more severe injuries.

Gaps in Knowledge

Biomaterials and gene therapy offer a unique way of controlling inflammation and regeneration after an SCI. However, many improvements remain critical for this technology to become fully efficacious in the clinic. Although a correlative link between IL10 treatment and improved SCI outcomes has been identified, some major caveats remain to be addressed. A better understanding of how IL10's therapeutic effects occur is necessary to illuminate its potential for success in a clinical setting.

First, IL10 may augment plasticity of spinal circuits, allowing intact circuits to compensate for those that are lost to primary and secondary damage. If plasticity underlies the behavioral improvements seen with IL10 treatment, then the age of an SCI victim will need to be considered when evaluating outcomes, because spinal cord plasticity decreases with age [156].

Second, decreased inflammation due to IL10 may result in earlier decompression than if inflammation were to take its natural time course. An earlier decompression would allow electrical signals to pass the injury site earlier, leading to less muscle atrophy. Thus, behavioral improvements would be due to the secondary effect of muscle preservation in the periphery and not due directly to tissue sparing within the central nervous system. Since the human spinal cord is about ten times the size of a mouse spinal cord, differences in tissue compressibility can therefore result in disparate and scale-dependent outcomes.

Third, though the effects of IL10 on tissue sparing and behavior have been well-documented in thoracic level injuries in rodents, the sparing of fine motor circuitry in a cervical level injury that is most relevant to human behavior needs to be demonstrated. These injury-level differences pose two important considerations. First, tissue composition varies at different spinal cord levels, with more cell bodies located in the cervical enlargement. If sparing is limited to only certain cell populations or parts of a neuron, then the therapeutic response may be dependent on the location and level of an injury. Second, locomotor function of the hindlimbs can be unilaterally initiated and sustained in both rodents and primates. However, due to a higher center of gravity, bipedal locomotion is much more difficult to maintain than quadrupedal locomotion. As a result, the roles of balance, proprioception, and fine motor control serve a greater contribution to primate behavior, so the individual responses to treatment of these different circuits must therefore be studied in greater detail. Consequently, successful translation will require a deeper understanding of IL10's mechanisms of action, such that therapeutic effects are not lost during the step from rodent to primate systems.

An understanding of the types of circuits formed by regenerated axons and whether regenerated axons – especially those of the CST – actually contribute to behavioral recovery seen

with treatment are critical pieces of information that must necessarily precede bench-to-bedside translation. Similarly for BDNF treatment, the roles of sparing, plasticity, and anti-inflammatory decompression may concurrently contribute to the improvements behavioral outcomes. Under the scenario that IL10's main effect is through sparing and BDNF's main effect is through regenerated axons, then a combinatorial therapy should be examined. For example, early tissue sparing might result in increased substrate from which regeneration can occur, thereby leading to further enhanced behavioral recovery than is possible with IL10 or BDNF alone.

Biomaterial implants and gene therapy are clearly extremely versatile tools with high therapeutic potentials, because they offer the ability to modify and create an environment that is supportive of tissue healing and regeneration. This thesis aims to explore and better define gaps in our current understanding of how biomaterials and gene therapy work to improve motor function, while simultaneously pushing the boundary of what our currently technology can accomplish.

Chapter 3 Lentiviral Interleukin-10 Gene Therapy Preserves Fine Motor Circuitry and Function After a Cervical Spinal Cord Injury in Male and Female Mice

Authors

Jessica Y. Chen, Emily J. Fu, Paras R. Patel, Hasan A. Sawan, Kayla A. Moss, Alexander J. Hostetler, Sarah E. Hocevar, Aileen J. Anderson, Cynthia A. Chestek, Lonnie D. Shea

Abstract

In mammals, spinal cord injuries often result in muscle paralysis through the apoptosis of lower motor neurons and denervation of neuromuscular junctions. Previous research shows that the inflammatory response to a spinal cord injury can cause additional tissue damage after the initial trauma. To modulate this inflammatory response, we delivered lentiviral anti-inflammatory interleukin-10, via loading onto an implantable biomaterial scaffold, into a left-sided hemisection at the C5 vertebra in mice. We hypothesized that improved behavioral outcomes associated with anti-inflammatory treatment are due to the sparing of fine motor circuit components. We examined behavioral recovery using a ladder beam, lower motor neuron apoptosis and muscle innervation using histology, and electromyogram recordings using intraspinal optogenetic stimulation at 2 weeks post-injury. Ladder beam analysis shows interleukin-10 treatment results in significant improvement of behavioral recovery at 2 and 12 weeks post-injury when compared to mice treated with a control virus. Histology shows interleukin-10 results in greater numbers of lower motor neurons and muscle innervation at 2 weeks post-injury. Furthermore, electromyogram recordings suggest that interleukin-10-treated animals have signal-to-noise ratios and peak-to-peak amplitudes more similar to that of uninjured controls than to that of control injured animals at 2 weeks post-injury. These data show that gene

therapy using anti-inflammatory interleukin-10 can significantly reduce lower motor neuron loss, muscle denervation, and subsequent motor deficits after a spinal cord injury. Together, these results suggest that early modulation of the injury response can preserve muscle function with long-lasting benefits.

Introduction

The loss of complex neural connections and inadequate nerve growth after a spinal cord injury (SCI) often results in permanent motor deficits or even complete paralysis [157]. Trauma can result in the apoptosis of lower motor neurons (LMNs), whose axons become detached from neuromuscular junctions (NMJs), leaving behind denervated motor endplates [109]. With sustained loss of neural input, these orphaned motor endplates will then release chemotactic signals to induce nearby, innervated NMJ axons to sprout growth cones [110, 111]. An orphaned motor endplate may then become re-innervated to form a functional NMJ. Alternatively, if the motor endplate remains denervated, it will disintegrate, the muscle fiber will atrophy, and paralysis will remain [113-117].

The early inflammatory response following trauma to the spinal cord can cause additional damage to neural tissues beyond the initial mechanical trauma [3, 158]. Immediately after the blood brain barrier is compromised, peripheral monocytes infiltrate the injury site and differentiate into macrophages that can exhibit phenotypes ranging from pro-inflammatory to anti-inflammatory. An inflammatory phenotype is highly linked to the secondary damage seen with an SCI, whereas the anti-inflammatory phenotype has been shown to encourage cell survival and tissue regeneration [4, 14]. Interleukin-10 (IL10) is an anti-inflammatory cytokine that is both expressed by macrophages and induces macrophage polarization towards an anti-inflammatory phenotype, which in turn results in a down-regulation of pro-apoptotic factors and

an upregulation of anti-apoptotic factors [29-31, 35]. In the absence of IL10, secondary damage is exacerbated [33]. Thus, shifting the post-injury response towards an anti-inflammatory phenotype has been a major target for therapeutic intervention.

The neuroprotective effects of IL10 treatment for an SCI have been investigated in several rodent studies. IL10 provides trophic support directly to neurons through the IL10 receptor [32], decreases post-injury inflammation [36], and increases myelination after a cervical SCI [159]. IL10 decreases lesion volume and apoptosis, while increasing behavioral recovery [36, 85, 160-166]. However, the majority of animal SCI studies are carried out in female subjects [85, 160-164, 166, 167], while most human SCIs occur in males [1]. Significant sex differences have been observed in immune responses after an SCI [168-170]. Furthermore, the majority of animal SCI studies are carried out at the thoracic level [85, 161-166], while cervical level injuries are estimated to make up about half of all human SCIs [7]. In contrast to thoracic spinal tissues, the cervical enlargement contains a greater proportion of circuitry that is responsible for fine motor control, and the impact of IL10 treatment of cervical SCI has not been investigated.

In this study, we examined immunomodulation after a cervical SCI and assessed the sparing of fine motor circuitry and functional recovery, using both male and female mice. A left C5 lateral hemisection was performed, resulting in loss of function of the left arm. The resected tissue was replaced with a biomaterial bridge made of poly(lactide-co-glycolide) (PLG) loaded with lentivirus encoding for IL10, while lentiviral firefly luciferase (FLuc) served as a control. Lentivirus delivery has previously been shown to induce localized and sustained transgene expression [5]. Lentiviral IL10 expression can shift post-SCI gene expression towards an anti-inflammatory profile [37, 171]. We initially analyzed behavioral recovery using a ladder beam at 2 and 12 weeks post-injury (wpi). Then, using immunohistochemistry, we quantified LMNs,

motor endplate densities, innervated NMJ densities, fraction of total NMJs that are innervated, and growth cone sprouting. We targeted the acromiotrapezius (ATZ) due to its topographical representation rostrally and throughout C5. In addition, we analyzed the flexor digitorum profundus & carpi ulnaris (FLX) together, due to their small size and topographical representation beginning in caudal C5 [108]. Finally, optogenetic stimulation was used to examine muscle activatability, which was quantified as a signal-to-noise ratio (SNR) and peak-to-peak (P2P) amplitude on an electromyogram (EMG). Our results show that early therapeutic intervention prevents some motor deficits by sparing the fine motor circuitry from secondary damage in both male and female mice.

Materials and Methods

Lentivirus Gene Delivery

Lentivirus containing pLenti-CMV-Luciferase or pLenti-CMV-IL10 was produced as previously described [36]. Briefly, HEK-293FT cells (American Type Culture Collection, Manassas, VA) were transfected with lentiviral packing vectors and plasmids of interest in Opti-MEM (Life Technologies, Carlsbad, CA, #31985-070) and Lipofectamine 2000 (Life Technologies, #11668-019). After 48hrs, the supernatant was collected and the virus was precipitated using PEG-It (Systems Biosciences, Palo Alto, CA, #LV825A-1) and stored at -80°C until use. Prior to surgery, 4e7 IFU of virus was loaded onto each PLG scaffold, which were fabricated as previously described using the gas foaming technique to fuse PLG particles into a matrix [36, 37, 106]. Using the particulate leaching technique, 63-106 μm NaCl served as sacrificial templates for pores to allow cell infiltration into the scaffold. A sugar mixture pulled into nine 150-250 μm diameter A-P parallel strands served as sacrificial templates for conduits to guide nerve growth [5, 50].

Animals and Surgery

All animal procedures were approved by the Institutional Animal Care and Use Committee at the University of Michigan. For histology and ladder beam, mice used were 2-3-month-old C57BL/6 (Jackson Laboratories, Bar Harbor, ME, #000664) at the time of injury. For optogenetics, mice used were 2-3-month-old Thy1-ChR2-YFP line 18 (Jackson Laboratories #007612) at the time of injury. Uninjured data is derived from age-, sex-, and genotype-matched controls at the time of sacrifice.

Mice were anesthetized under 2% isoflurane. The surgery site was then shaved and disinfected with iodine and 70% ethanol. Bupivacaine (0.8ml/kg) was delivered locally to the incision site, and a C5 laminectomy was performed. Using a microfeather microscalpel (VWR, Radnor, PA, #72045-15), a left lateral hemisection of 1mm length (A-P) was performed at C5. The spinal tissue was excised and replaced with a lentivirus-loaded scaffold. Then the injury site was covered using GELFOAM (Pfizer, New York, NY), the overlying muscle was sutured using 5-0 Chromic Gut (Henry Schein, Melville, NY, #101-8824), and the skin was stapled. Mice received buprenorphine (0.1mg/kg) twice daily for 3 days, lactated ringer's solution fluid supplement (5ml/100g) daily for 5 days, and enrofloxacin (2.5mg/kg) daily for 2 weeks.

Behavioral Analysis

C57BL/6 females only, due to persistent bladder issues in males, were trained to walk across a ladder beam consisting of 50+ rungs prior to surgery as previously described [172]. After surgery, at 2 and 12 wpi, animals were placed on the ladder beam and coerced to walk across while being recorded on video. A minimum of 3 trials was completed for each animal at each time point. The videos were randomized among a total of four individuals such that each video was quantified by two counters who were blinded to the treatment condition. Then each

video's quantifications were averaged between the two counters. A placement could be scored as 1) a complete placement with all toes facing forward and the palm on the rung, 2) a partial placement where the toes may be curled or the palm may not be centered though the limb is still weight-bearing, or 3) skipped rungs where the flanking rungs are placements. All others, such as misses or slips, were not counted. Examples can be seen in Figure 5.

Histological Analyses

At 2 wpi, spinal tissues and arm muscles were extracted, flash frozen in isopentane on dry ice, then cryosectioned at 12μm in the transverse plane and 14μm in the longitudinal plane, respectively. Spinal and muscle tissues were stained following a standard immunohistochemistry protocol with fixation and without fixation in 4% paraformaldehyde, respectively. Antibodies used were mouse anti-NeuN (1:250, Millipore, Burlington, MA, #MAB377) for mature neurons, chicken anti-NF200 (1:250, AVES Labs, Davis, CA, #NFH) for neurofilaments, anti-bungarotoxin conjugated to Alexa Fluor 647 (1:500, Thermo Fisher, Waltham, MA, #B35450) for motor endplates, and rabbit anti-GAP43 (1:100, Millipore, Burlington, MA, #AB5220) for growth cones. Secondary antibodies were Alexa Fluor 647 donkey anti-mouse (1:1000, Jackson ImmunoResearch, West Grove, PA #715-606-150), Alexa Fluor 488 goat anti-chicken (1:1000, Jackson ImmunoResearch, #103-547-008), and Alexa Fluor 594 goat anti-rabbit (1:1000, Jackson ImmunoResearch, #111-587-003).

Tissues were imaged using a Zeiss Axio Observer.Z1 microscope at 10X and processed in FIJI [173]. The analyze particles function (0.5-1 circularity, exclude on edges) in FIJI was utilized to count cells of 100-250 μm^2 and 250-1100 μm^2 on images that had a threshold established by a single observer who was blinded to the experimental condition. A minimum total of 300 neurons across a minimum of 4 spinal cord sections from each spinal cord sample

was quantified. Total motor endplate density, innervated motor endplate density, fraction of innervated motor endplates, and fraction of motor endplates with a growth cone nearby were quantified and averaged across two counters who were blinded to the experimental condition. If an NF200+ or GAP43+ axon was colocalized or <1 axon diameter away from a motor endplate, then it would be considered innervated or in the process of being re-innervated, respectively. A minimum total of 150 motor endplates across a minimum of 3 muscle sections from each muscle sample was quantified.

Optogenetic Stimulation

The spinal column of Thy1-ChR2-YFP mice anesthetized under 2% isoflurane was exposed, and a C4-C6 laminectomy was performed from the dorsal side. The dura mater over C4-C6 was removed to allow insertion of a 1mm long LED probe (Plexon, Dallas, TX, #OPT/FS-Flat-110/125-1L) into the left C4, midway between the lateral edge of the spinal cord and the midline. Optical stimulation was delivered using a PlexBright Controller to drive a 465nm HELIOS headstage (Plexon, #OPT/LED_Blue_HELIOS_LC_Kit) in a faraday cage. The optical stimulation parameters were 20ms pulse width at 1Hz with a power of 0.04mW for a minimum of 3 minutes per animal.

EMG Data Acquisition and Processing

Digital out and reference signals from the PlexBright Controller were sent to a headstage (Tucker-Davis Technologies, Alachua, FL, #RA16AC) that was connected to a pre-amplifier (Tucker-Davis Technologies #RA16PA), which converted the inputted electrical signal into an outputted optical signal. To gain access to the muscle, small incisions were made in the skin and needle electrodes (Natus Neurology, Pleasanton, CA, #019-475400) were dually implanted into the left and right ATZ and FLX muscles. A single electrode in the left back ankle served as the

reference signal. EMG and reference signals from the animal were connected to a second headstage and a second pre-amplifier. The optical outputs from each pre-amplifier were recorded by the same RX7 system (Tucker-Davis Technologies). A schematic for the equipment setup can be seen in **Figure 10A** and an example EMG recording can be seen in **Figure 10B**.

Signals from both headstages were acquired at a synchronized rate of 24,414Hz with bandpass frequencies of 2.2Hz-7.5kHz. After acquisition, the data was converted to MATLAB® format using custom scripts. Next, the differential EMG electrode pairs were subtracted from each other and then band passed between 100-500Hz. To calculate the SNR for each muscle, a threshold was applied to the digital out signal representing the optical stimulation to determine the on and off times of the stimulation. Then, these times were used to calculate the root mean square values of the EMG signal during activation (stimulation on) and background (stimulation off). The ratio of the two values (on vs. off) was then used to calculate the SNR. To calculate the average P2P amplitude for each muscle, the maximum-to-minimum difference for each stimulation on time was determined, then averaged across all the stimulation on times for the length of that recording session.

Results

Functional Recovery with IL10 Expression

Initial studies analyzed the behavioral response following a penetrating injury to the cervical spinal cord. A left-sided hemisection to the cervical enlargement at C5 allowed isolation of SCI-induced motor deficits to only the left forelimb. The injury level, injury sidedness, and difficulty of placing a weight-bearing limb onto a ladder beam rung allowed quantification of movement that requires significant fine motor control. Previous reports show uninjured control animals average 50 placements [172]. Animals receiving a bridge with a lentivirus encoding

IL10 averaged 12.3 and 10.4 placements at 2 and 12 wpi, respectively. Animals receiving a bridge with a lentivirus encoding FLuc averaged 8.7 and 6.2 left forelimb placements at 2 and 12 wpi, respectively. A two-way ANOVA indicates that IL10 significantly increased placements relative to FLuc ($p = 0.037$), while no differences in performance were observed over time ($p = 0.24$) or for interaction between time and virus condition ($p = 0.87$) (**Figure 5**).

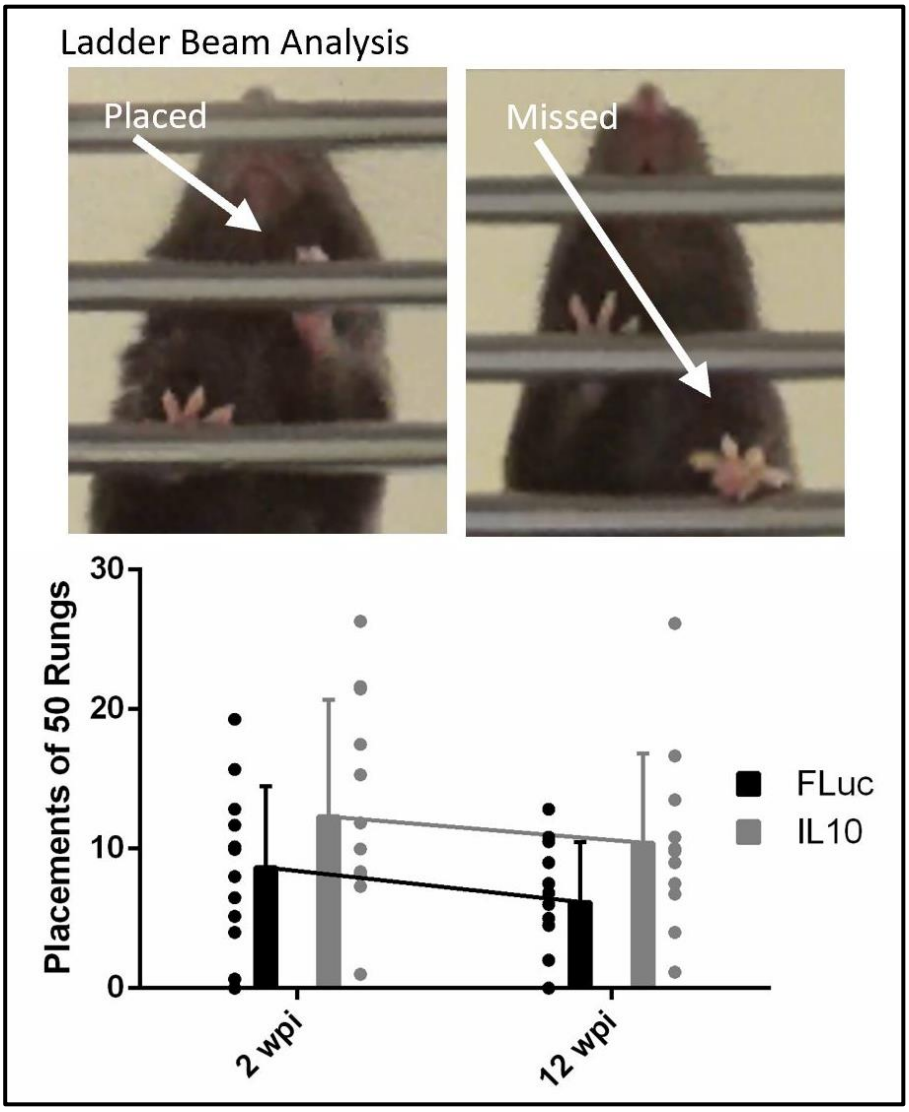

Figure 5. Paw placements (top) and counts (bottom) show IL10-treated animals perform significantly better when compared to FLuc-treated animals Error bars are ± SD. n = 12 – 13 animals/condition. Two-way ANOVA ($p < 0.05$ for virus condition).

Neuronal and NMJ Sparing with IL10

Inflammation following trauma can result in the apoptosis of neurons, and we thus quantified peri-injury neuronal density. NeuN+ neuron cell bodies range between 100-1100 μm^2, with LMNs having larger sizes (250-1100 μm^2) than interneurons (100-250 μm^2) [174]. Histological analyses of ipsilateral, peri-injury, caudal tissues at 2 wpi showed that animals treated with IL10 had significantly more interneurons and total neurons per section than animals treated with FLuc (**Figure 6**). Since both the injured and contralateral side of FLuc-treated animals trended towards decreased neuron densities for all sizes of neurons analyzed, we added age- and sex-matched, uninjured controls for all subsequent experiments.

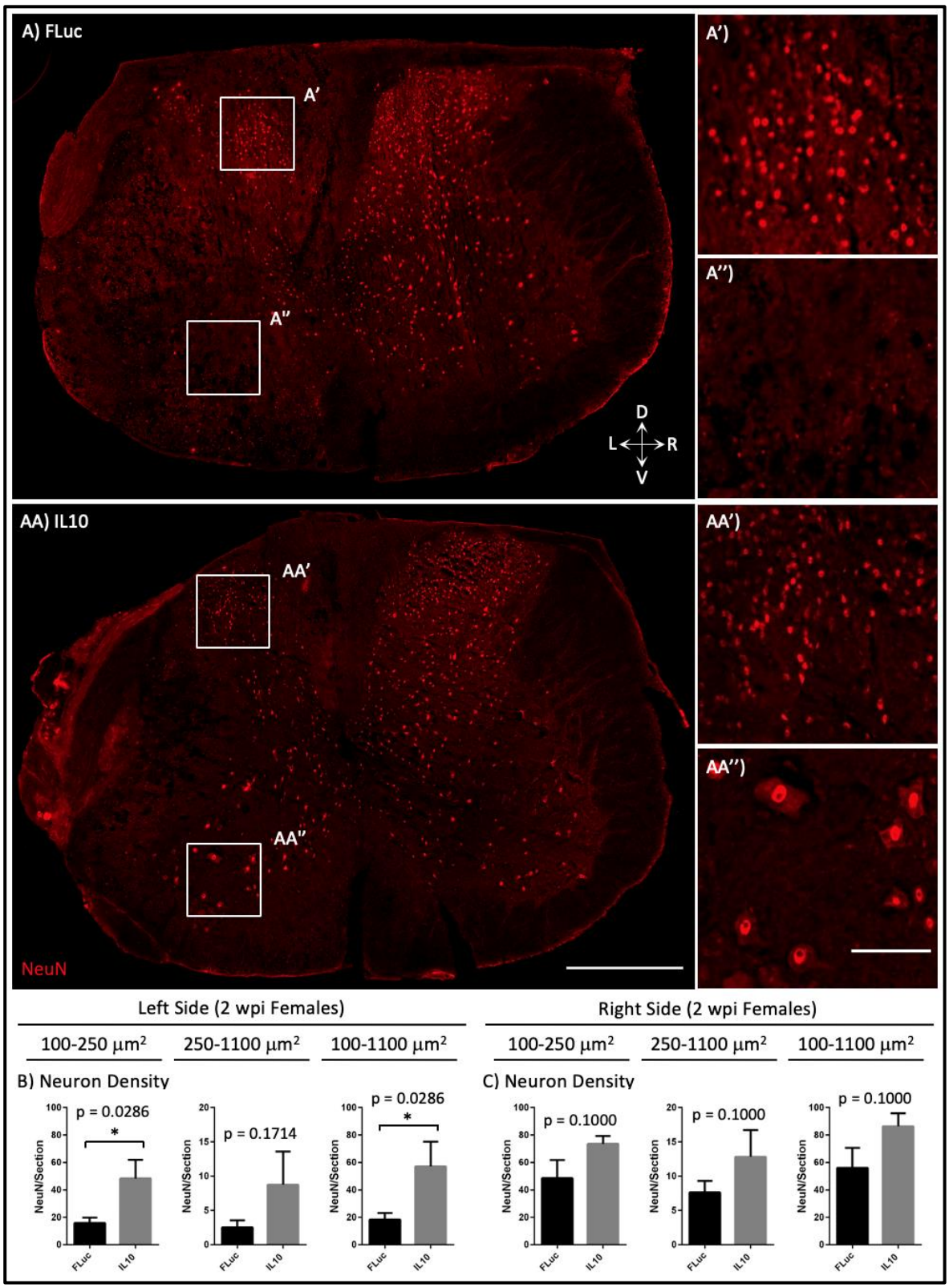

*Figure 6. Representative images of mature neurons (NeuN) per section for FLuc (A) and IL10 (AA), 100-250 μm^2 size neurons (A', AA'), and 250-1100 μm^2 size neurons (A'', AA'') are shown. Quantifications of neurons normalized to each section for the left (B) and right (C) side are shown for each size range for 2 wpi females. Error bars are ± SEM. n = 4 animals/condition. Mann-Whitney test *p < 0.05. Scale bar = 500µm (A, AA), 100µm (A', A'', AA', AA'').*

Next, we analyzed sparing in the peripheral nervous system through the quantification of motor endplate density and NMJ innervation status. The NMJs were characterized as innervated (overlap of NF200+ neurofilament (NFM) and bungarotoxin (BGT)) (**Figure 7A**), denervated (separation of NFM and BGT) (**Figure 7B**), and reinnervated (overlap of BGT and growth-associated protein 43 (GAP43)) (**Figure 7C**).

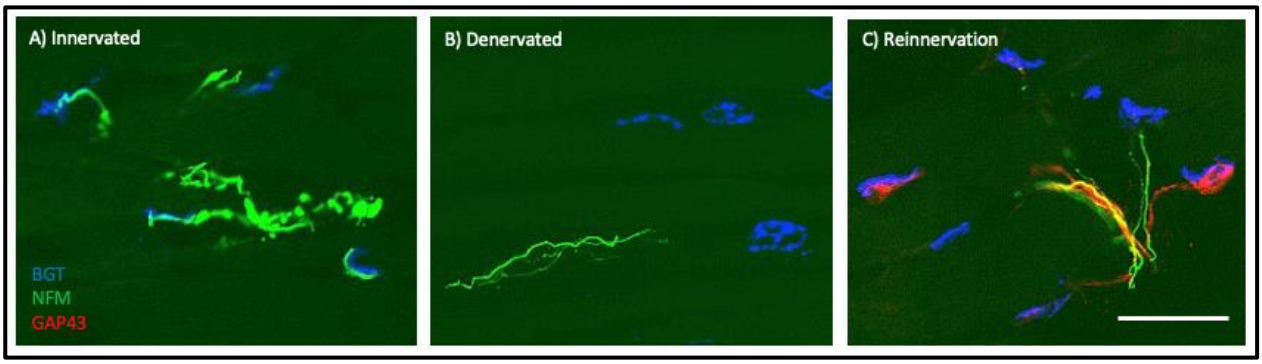

Figure 7. Tissue sections were stained for bungarotoxin (BGT) for motor endplates, neurofilament (NFM) for axons, and growth-associated protein 43 (GAP43) for growth cones. Representative images of NMJs that are (A) innervated, (B) denervated, or being (C) reinnervated are shown. Scale bar = 50 μm.

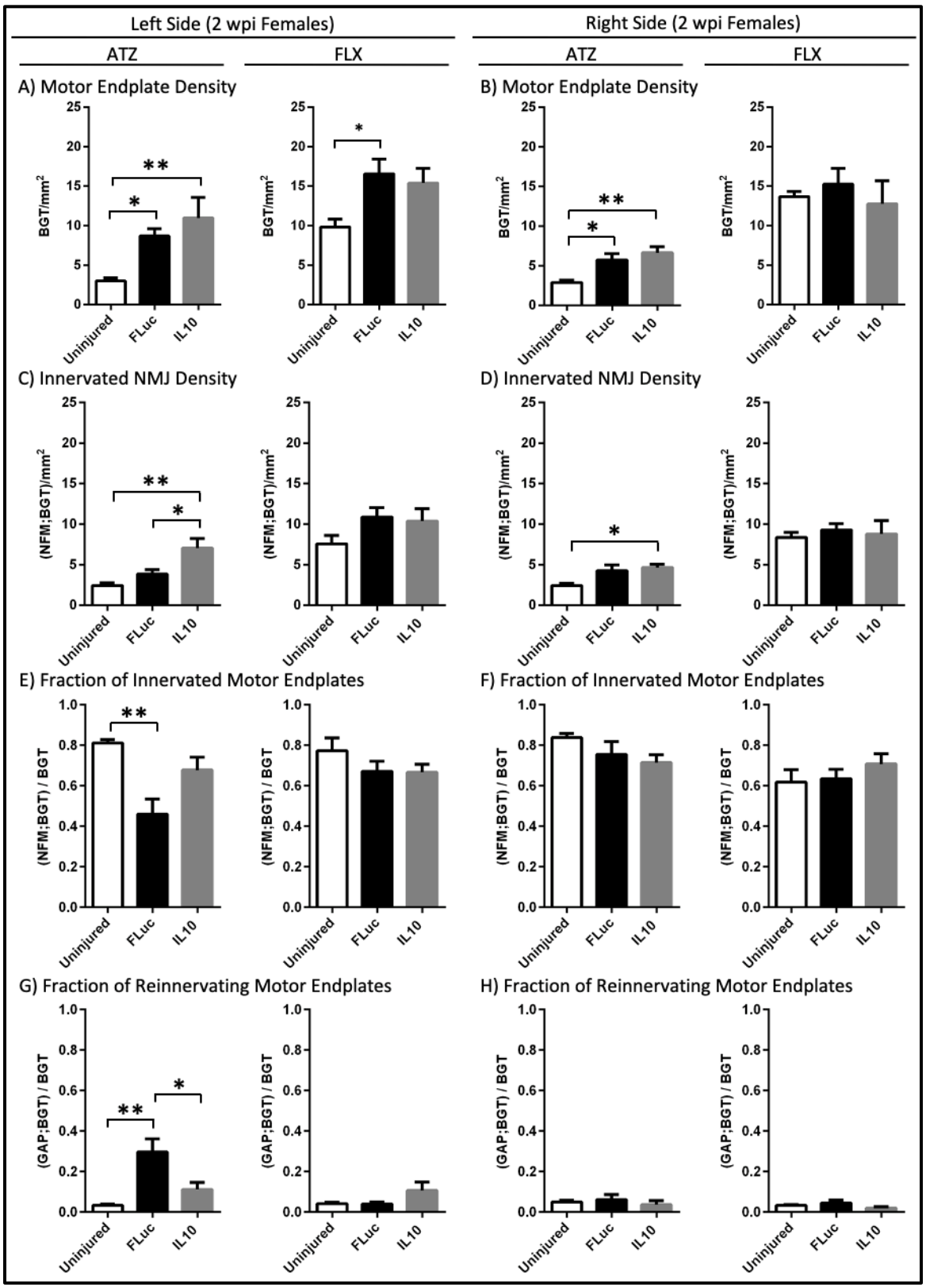

*Figure 8. Quantifications of motor endplate density normalized to muscle area (A, B), innervated NMJ density normalized to muscle area (C, D), fraction of total motor endplates that are innervated (E, F), and fraction of total motor endplates that are being reinnervated (G, H) are shown for 2 wpi females. Error bars are ± SEM. n = 5 - 6 animals/condition. One-Way ANOVA with Tukey Post-Hoc *p < 0.05, **p < 0.01.*

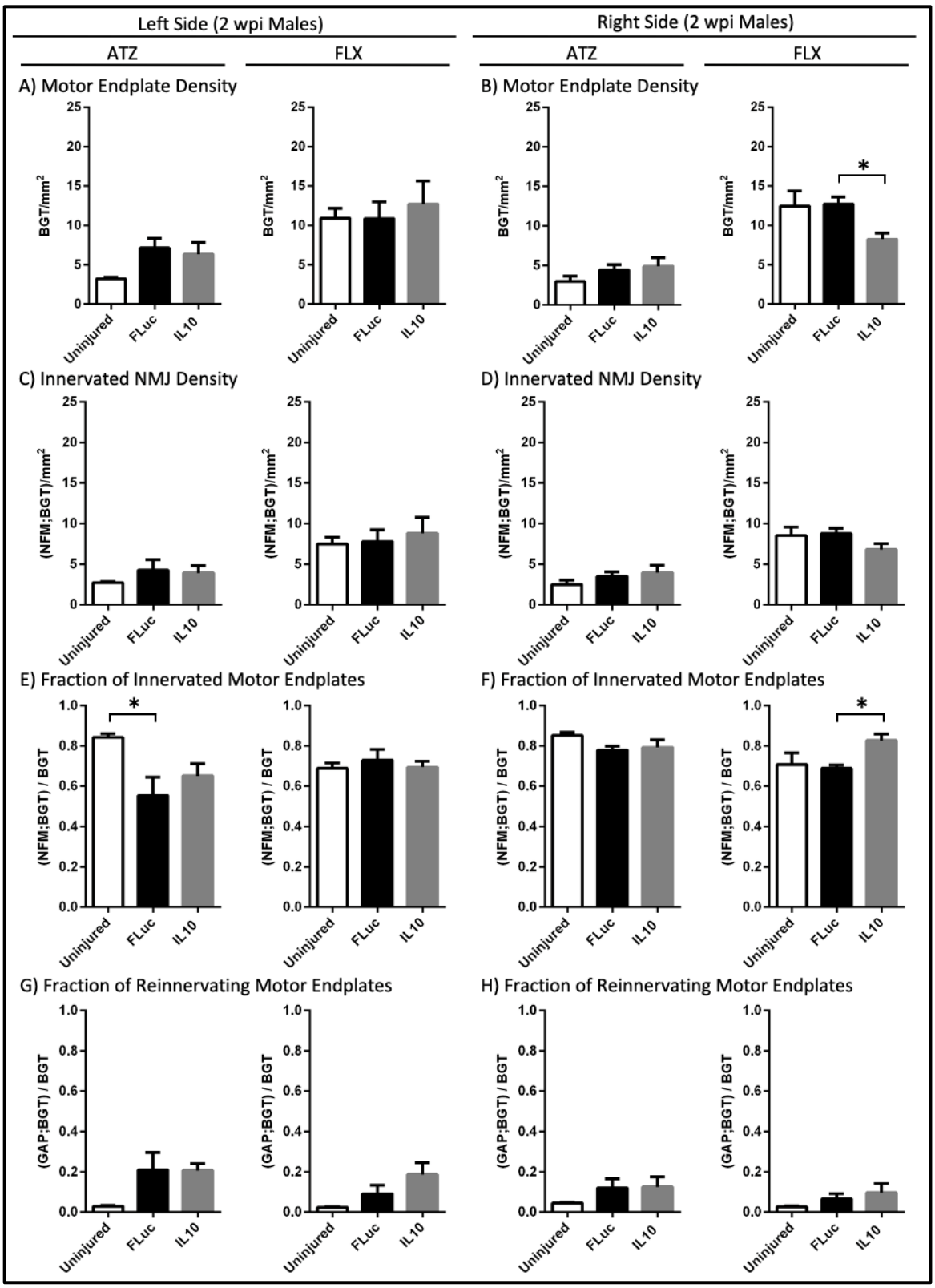

*Figure 9. Quantifications of motor endplate density normalized to muscle area (A, B), innervated NMJ density normalized to muscle area (C, D), fraction of total motor endplates that are innervated (E, F), and fraction of total motor endplates that are being reinnervated (G, H) are shown for 2 wpi males. Error bars are ± SEM. n = 5 - 6 animals/condition. One-Way ANOVA with Tukey Post-Hoc *p < 0.05.*

For both females (**Figure 8B, D, F, H**) and males (**Figure 9B, D, F, H**), a few significant differences were observed between conditions in the contralateral side, thereby supporting the use of an age- and sex-matched uninjured control. Additionally, for both female and male FLX muscles, the analysis of the NMJs largely showed no significant difference between the experimental conditions and uninjured controls. The lack of difference between injury and control suggests that the injury was consistently rostral to where FLX muscle innervation began.

In the left ATZ of females, a significant increase in motor endplate and innervated NMJ density per muscle area were observed in animals treated with either IL10 or FLuc relative to control uninjured animals (**Figure 8A, C**). This result is consistent with previous reports showing that motor endplates will undergo fragmentation after a denervating event, resulting in an apparent increase in motor endplate density prior to the onset of muscle atrophy [175]. To account for fragmentation, we quantified the fraction of total motor endplates that are innervated and found that FLuc-treated animals had significantly decreased innervation when compared to that of control uninjured animals (**Figure 8E**). Quantification of motor endplates colocalizing with growth cones showed that animals treated with FLuc also had the highest level of reinnervation (**Figure 8G**). Since no difference in reinnervation or fraction of innervated motor endplates could be observed between IL10-treated and uninjured control animals, these data suggested IL10 spared more NMJs from denervation (**Figure 8E, G**).

Overall, the differences observed for females (**Figure 8**) were also seen in males, but to a lesser extent (**Figure 9**). The left ATZ in males treated with either IL10 or FLuc trended toward an increase in motor endplate and innervated NMJ densities (**Figure 9A, C**). As with females, male mice treated with FLuc, but not IL10, had a significant decrease in their fraction of innervated motor endplates when compared to control uninjured animals (**Figure 9E**). Animals

treated with either IL10 or FLuc also trended towards an increase in their fraction of reinnervating motor endplates when compared to control uninjured animals (**Figure 9G**). All p-values are reported in **Table 1**.

Figure #	One-Way ANOVA p-value	Tukey Post-Hoc p-value		
		Uninjured vs. FLuc	Uninjured vs. IL10	FLuc vs. IL10
8A (ATZ)	0.0099	0.0498	0.0093	0.5516
8A (FLX)	0.0312	0.0318	0.0944	0.8703
8B (ATZ)	0.0057	0.0262	0.0060	0.6114
8B (FLX)	0.6898	0.8535	0.9502	0.6750
8C (ATZ)	0.0034	0.4107	0.0031	0.0253
8C (FLX)	0.1744	0.1788	0.3070	0.9542
8D (ATZ)	0.0299	0.0715	0.0350	0.8618
8D (FLX)	0.8300	0.8166	0.9627	0.9398
8E (ATZ)	0.0040	0.0033	0.3289	0.0586
8E (FLX)	0.3022	0.3645	0.3606	0.9972
8F (ATZ)	0.2239	0.4378	0.2102	0.8188
8F (FLX)	0.4727	0.9717	0.4871	0.5896
8G (ATZ)	0.0037	0.0035	0.4920	0.0342
8G (FLX)	0.1184	0.9991	0.1793	0.1465
8H (ATZ)	0.6967	0.9157	0.8990	0.6726
8H (FLX)	0.2711	0.6793	0.7029	0.2429
9A (ATZ)	0.0981	0.0976	0.2081	0.8830
9A (FLX)	0.8125	> 0.9999	0.8545	0.8346
9B (ATZ)	0.2882	0.4701	0.2771	0.9090
9B (FLX)	0.0324	0.9885	0.0729	0.0445
9C (ATZ)	0.5309	0.5249	0.6694	0.9653
9C (FLX)	0.8221	0.9888	0.8263	0.8858
9D (ATZ)	0.3750	0.5983	0.3528	0.8872
9D (FLX)	0.2022	0.9758	0.3373	0.2200
9E (ATZ)	0.0334	0.0277	0.1648	0.5640
9E (FLX)	0.7407	0.7623	0.9936	0.8060
9F (ATZ)	0.1895	0.1913	0.3198	0.9313
9F (FLX)	0.0357	0.9287	0.1008	0.0411
9G (ATZ)	0.0808	0.1106	0.1153	0.9997
9G (FLX)	0.0689	0.5723	0.0599	0.2928
9H (ATZ)	0.3778	0.4569	0.4137	0.9961
9H (FLX)	0.3576	0.6860	0.3260	0.7781

*Table 1. One-Way ANOVA p-values and Tukey Post-Hoc p-values associated with **Figure 8** and **Figure 9**.*

Sparing of Muscle Activation with IL10

Next, we tested the hypothesis that NMJ differences identified by histology influence muscle activation characteristics, which could be analyzed using electrophysiology. Denervation of an NMJ releases factors that can induce sprouting of nearby axons [110, 111]. If a denervated NMJ becomes captured by a new motor unit, then stimulation of the adopting motor unit will result in an increased contractile force that is correlated with the amplitude of a compound action potential, which can be measured by an EMG. If a denervated NMJ remains orphaned, then stimulation of the motor unit that formerly owned that NMJ will show a decrease in the amplitude of its compound action potential [113-117]. Therefore, we quantified the compound action potential as a P2P amplitude after optogenetic stimulation of channelrhodopsin positive C4 axons. Additionally, we quantified the SNR because, though not technically "noise," background signals due to spontaneous fibrillations are a common characteristic of denervated muscles and can indicate damage to the motor circuitry independent of P2P changes.

No statistically significant differences in P2P and SNR values were observed between IL10-treated and uninjured control animals for both males and females, and for both the left ATZ and FLX muscles at 2 wpi (**Figure 11A, B, E, F**), suggesting IL10 spared the motor circuitry from secondary damage. Meanwhile, females treated with FLuc had significantly lower left ATZ SNRs when compared to control uninjured animals (Figure 11), whereas males treated with FLuc had significantly lower left ATZ P2Ps and SNRs when compared to animals treated with IL10 (**Figure 11E, F**). FLuc-treated males also had significantly lower left ATZ P2Ps when compared to uninjured control males (**Figure 11E**). Together, these data show that the profound detrimental effects an SCI has on muscle activation, which can be identified in EMG recordings after optogenetic stimulation, can be alleviated using anti-inflammatory IL10 gene therapy.

Finally, no trends or statistically significant differences could be observed in the contralateral side (**Figure 11C, D, G, H**), which all had low values, suggesting that the optogenetic stimulation light was contained within the left C4. All p-values are reported in **Table 2**.

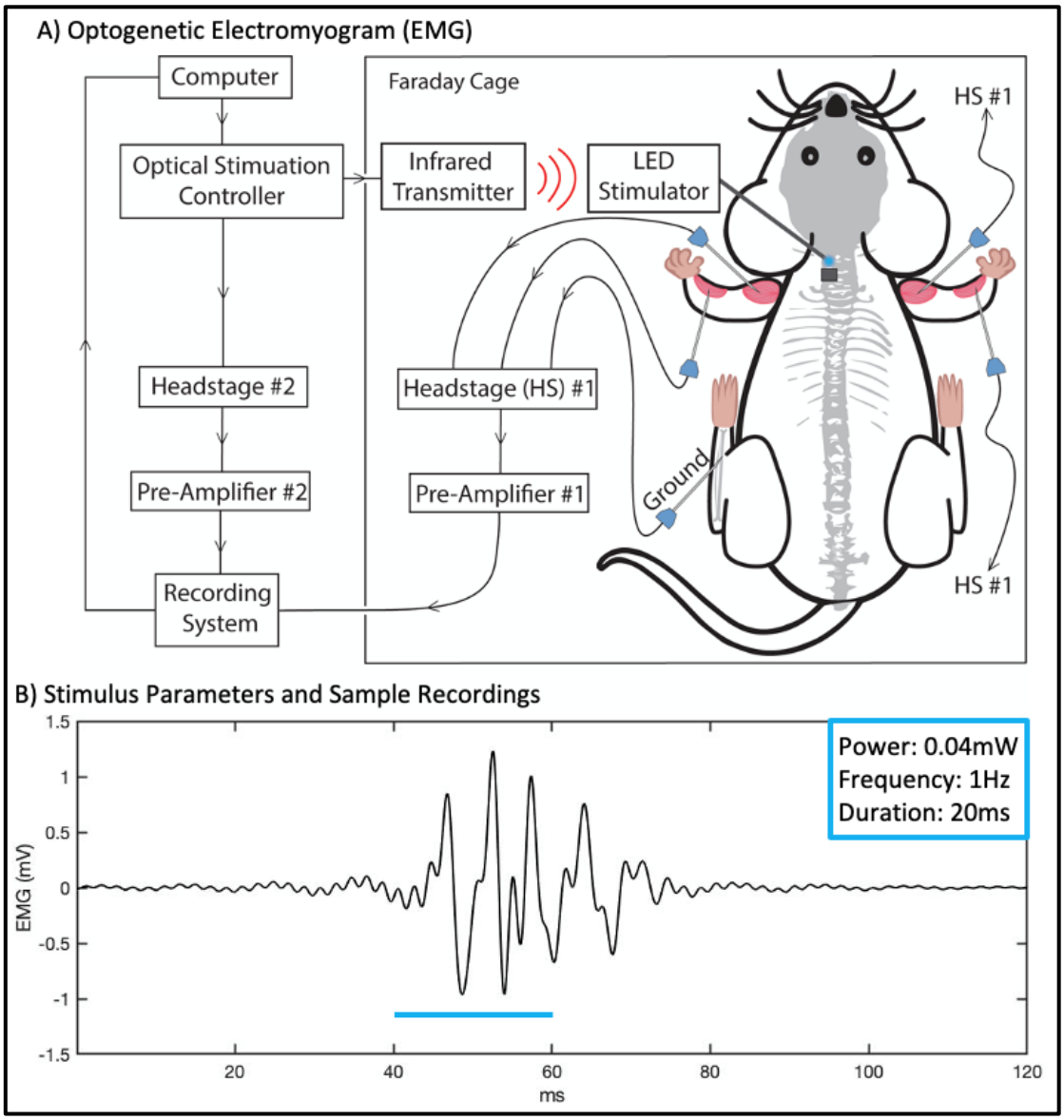

Figure 10. Schematic of the equipment setup (A) for optogenetically-evoked electromyogram recordings is shown, as well as the stimulus parameters (20ms pulses, 0.04mW, 3min, 1Hz) and a representative EMG trace (B).

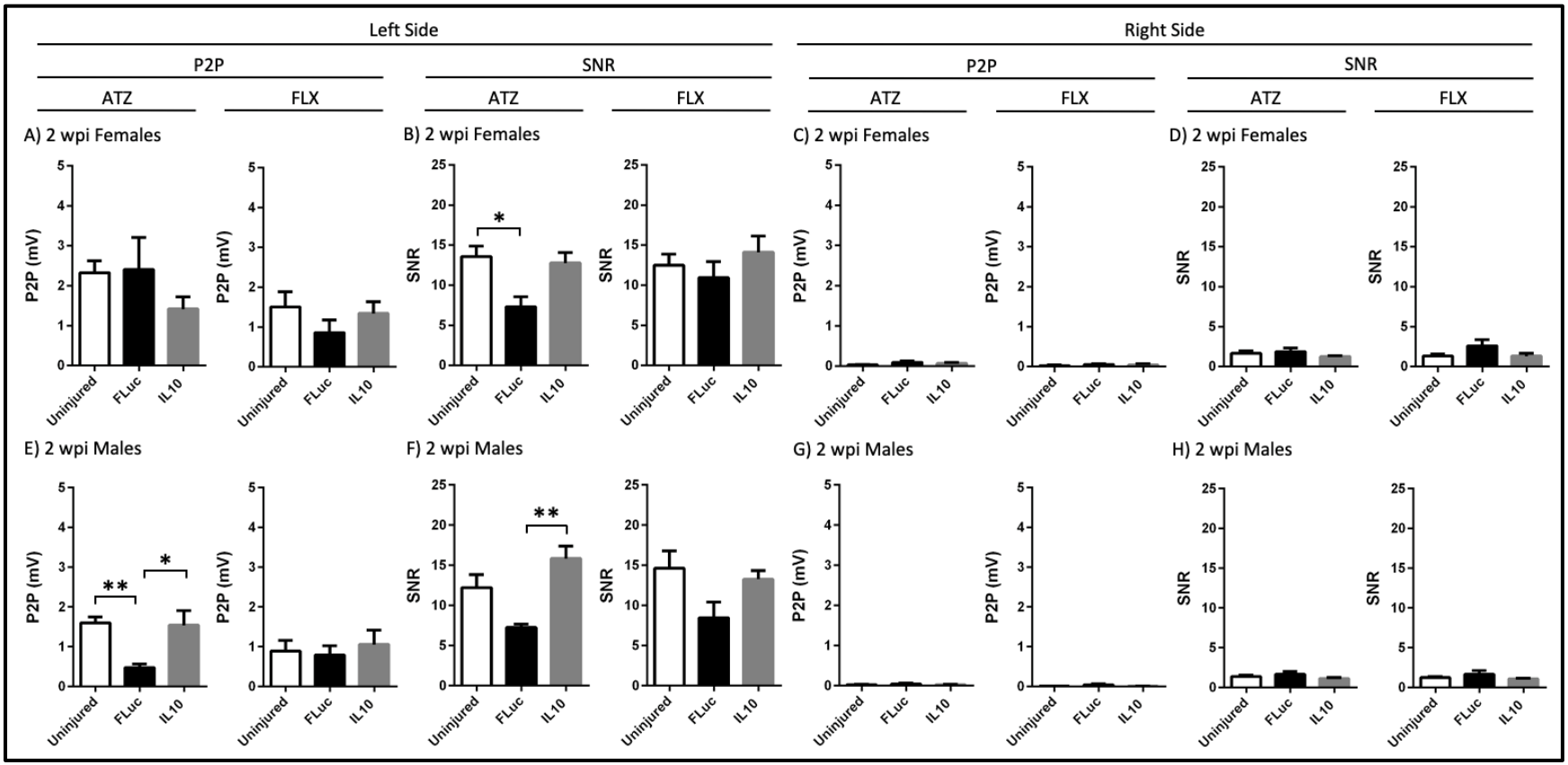

*Figure 11. The peak-to-peak (A, C, E, G) and signal-to-noise ratios (B, D, F, H) for 2 wpi females (A, B, C, D), 2 wpi males (E, F, G, H) was quantified for the ATZ and FLX muscles. Error bars are ± SEM. n = 4 - 8 animals/condition. One-Way ANOVA with Tukey Post-Hoc *p < 0.05, **p < 0.01.*

Figure #	One-Way ANOVA p-value	Tukey Post-Hoc p-value		
		Uninjured vs. FLuc	Uninjured vs. IL10	FLuc vs. IL10
11C (ATZ)	0.2207	0.9914	0.2591	0.3220
11C (FLX)	0.5117	0.4834	0.9390	0.6881
11D (ATZ)	0.0207	0.0193	0.9010	0.0532
11D (FLX)	0.5296	0.8287	0.7701	0.5060
11E (ATZ)	0.1146	0.1129	0.3678	0.6649
11E (FLX)	0.7058	0.7199	0.8262	0.9674
11F (ATZ)	0.4284	0.8900	0.5942	0.4348
11F (FLX)	0.1101	0.1239	> 0.9999	0.1492
11G (ATZ)	0.0052	0.0066	0.9763	0.0162
11G (FLX)	0.8323	0.9659	0.9160	0.8206
11H (ATZ)	0.0045	0.0607	0.1991	0.0035
11H (FLX)	0.1001	0.0917	0.8698	0.2602
11I (ATZ)	0.4795	0.5936	0.9606	0.4900
11I (FLX)	0.0545	0.0685	> 0.9999	0.0961
11J (ATZ)	0.2971	0.6497	0.6737	0.2670
11J (FLX)	0.2472	0.4042	0.8741	0.2440

*Table 2. One-Way ANOVA p-values and Tukey Post-Hoc p-values associated with **Figure 11**.*

Discussion

Our studies examined the potential for anti-inflammatory stimuli to enhance the fine motor circuitry and muscle activation in a cervical SCI model. The studies reported here validate that lentiviral IL10 gene therapy via a PLG implant into a left-sided, cervical SCI is associated with significantly improved performance of the left arm, as observed on a ladder beam. A number of groups have reported that IL10 treatment after a thoracic SCI can lead to intraspinal sparing of neurons, axons, and lesion size that is associated with improved locomotor function [85, 161-166]. We have also previously demonstrated in a left-sided, thoracic SCI that IL10 can shift the inflammatory milieu toward a pro-regenerative phenotype, which was associated with significantly improved locomotor function [37, 171] and consistent with the results here in the

cervical model. Thoracic injuries that employ behavioral tests such as the basso mouse scale for locomotion, which is controlled by central pattern generators (CPGs) that can be unilaterally activated to initiate bilateral locomotor behavior, may not fully capture the deficit from the unilateral injury. In contrast, cervical injuries are assessed through analysis of fine motor control. which is controlled unilaterally [176]. Maintenance of fine motor control is also particularly relevant to humans, as we rely on forelimbs to a greater extent than rodents. Therefore, our studies provide further insight into IL10's therapeutic benefits on the fine motor circuitry, in contrast to previous behavioral tests on hindlimb function in which CPGs and reflexes play a larger role.

Additionally, we demonstrate that IL10 expression within the spinal cord impacts processes in the periphery. Specifically, examination of muscles innervated at the level of injury indicated that IL10 decreased NMJ denervation and prevented the pathological increase in motor unit and spontaneous fibrillations in those same muscles. In mice, the ATZ is innervated by LMNs whose cell bodies reside between C2-C6 [108]. Within minutes after an injury, direct loss of the LMN cell body, such as removal via hemisection, can result in Wallerian degeneration of the axon and NMJ denervation [177, 178]. This first denervating event is likely unavoidable because the majority of hemisected LMN cell bodies from C5 were innervating the left ATZ. Later, peri-injury LMNs can undergo apoptosis that peaks at 3 days post injury in the highly inflammatory post-SCI environment, followed by axon degeneration and NMJ denervation [3, 179, 180]. This second denervating event is the target of our anti-inflammatory treatment. After a denervating event, motor endplates will undergo fragmentation [175, 181, 182]. The cumulative effects of direct removal of the LMN cell body and secondary damage due to inflammation can be seen most profoundly in the 2 wpi left ATZ of animals treated with FLuc, which had a

significant increase in motor endplate density that reflects fragmentation and a significant decrease in the fraction of total motor endplates that are innervated when compared to uninjured control animals. Meanwhile, although the 2 wpi left ATZ of IL10-treated animals also showed significant motor endplate fragmentation, the fraction of total motor endplates that are innervated remained comparable to that of uninjured controls. Since animals treated with IL10 also had far fewer growth cones than animals treated with FLuc, suggesting a decreased need for reinnervation, together these data indicate a decrease in injury severity that is likely due to our anti-inflammatory treatment. We therefore identify IL10-induced sparing of NMJs in the left ATZ as a major contributor to improved fine motor control after a cervical SCI.

We report that IL10 treatment was effective in both male and female mice, though with some differences. All previous studies for delivery of IL10 used female rodents [85, 159-164, 166, 171], except for one that did not indicate the sex of their animals [165]. Since differences in the neuroinflammatory response and locomotor recovery between male and female mice have been identified [183], IL10 treatment could potentially have disparate effects in each sex. For all the electrophysiological measures, no difference could be found between uninjured and IL10-treated animals, further supporting therapeutic benefits of IL10 in both sexes. Interestingly, control injury significantly reduced the P2P of the left ATZ, reflecting a decrease in motor unit size due to injury, in males but not in females. Since we found females treated with FLuc had significantly increased reinnervation, then reestablishment of a normal motor unit size might account for the apparently normal P2P seen in the left ATZ. We therefore suspect that a timepoint slightly earlier than 2wpi might have shown a decreased P2P in the female left ATZ, whereas a slightly later timepoint might have shown an increased P2P. Whether or not females have more or accelerated reinnervation relative to males remains to be determined. We do not

anticipate that the normal P2P of the ATZ in females treated with FLuc reflects a lack of pathological outcomes, because increased pathological fibrillations explain why the SNR in females was decreased despite no observable reduction in the P2P values. Additionally, while the electrophysiological effects of IL10 in males were clear, males showed fewer histological differences between conditions. Since all experiments were carried out in C57/BL6 background mice, and increased testosterone has been linked with increased neutrophil activation and decreased functional outcomes [184, 185], we suspect that the observed sex differences reflect mechanistic differences in the injury response.

While tissue sparing is associated with preservation of function as measured by behavior and by optical stimulation at 2 wpi, no additional behavioral improvements were observed at 12 wpi. Hemisected intraspinal reflex and locomotor circuits will inevitably result in the loss of some synchronized muscle activation that is necessary for normal gait to occur. Additionally, increases in motor unit size due to reinnervation will decrease an animal's control over their contractile force, such that the ratio of cognitive effort necessary to elicit a specific force will be shifted during fine motor movements [186]. If a muscle or neuron becomes inappropriately reinnervated after injury, the resulting synkinesis can further disrupt the synchronized muscle activation that is necessary for coordinated movement. Therefore, though sparing the motor circuitry by decreasing secondary damage due to inflammation can prevent some of the motor deficits that often results from an SCI, future studies might need to focus on the specificity of circuit reconnection in order for proper behavioral recovery to occur.

Conclusions

This study utilizes a left-sided, cervical level SCI to demonstrate that lentiviral IL10 can prevent some motor deficits from forming in the left arm. Intraspinal expression of IL10 can

preserve NMJ innervation in the peripheral nervous system. Using optogenetic stimulation of C4 axons that originate from channelrhodopsin positive layer V neurons, we were able to examine muscle activation due solely to the fine motor circuitry and demonstrate that IL10 treatment can prevent pathological EMG signals in injury-affected muscles. Furthermore, these findings were mostly consistent in both male and female mice indicating potential applicability for both sexes. Collectively, our results indicate that early immunomodulatory intervention can yield long-term benefits.

Chapter 4 Examination of Muscle Fatigue and the Electrical Activity of Regenerated Axons After a Spinal Cord Injury Treated with Biomaterial Implantation and Gene Therapy

Authors

Jessica Y. Chen, Alexander J. Hostetler, Sarah E. Hocevar, Paras R. Patel, Emily J. Fu, Kayla A. Moss, Longshun Li, Hasan A Sawan, Aileen J. Anderson, Cynthia A Chestek, Lonnie D. Shea

Abstract

A traumatic spinal cord injury and subsequent neuroinflammation cause permanent damage to spinal tissues. While progress has been made to decrease inflammation, increase regeneration, decrease glial scarring, and increase myelination, full return of motor function remains elusive in preclinical studies. The myriad of tissue structure disruptions that occur along with a spinal cord injury necessitates a combinatorial therapeutic approach. The studies presented here examine the individual and combined effects of interleukin-10 and brain-derived neurotrophic factor gene therapy on different aspects of the fine motor circuitry, including muscle innervation and fatigue, axon regeneration, and signal transmission in regenerated axons. Histological and electromyogram analyses at 2 weeks post-injury suggest interleukin-10 alone and in combination with brain-derived neurotrophic factor have a similar, non-additive, sparing effect on neuromuscular junction innervation. However, by 12 weeks post-injury, innervation differences can no longer be observed. Preliminary results examining prolonged muscle activation suggest post-injury differences exist in muscle fatigability, which may be preventable with gene therapy treatment. Ongoing histological studies aim to corroborate these electrophysiological findings. Within the spinal cord, quantification of axon regeneration at 2

weeks post-injury suggests interleukin-10 alone and in combination with brain-derived neurotrophic factor also have a similar, non-additive, effect on promoting axon regeneration. 3D imaging in cleared spinal tissues show that regenerated axons can be traced across the entire injury site, while intraspinal recordings shows that these axons are electrically active. These studies demonstrate that early tissue sparing due to decreased inflammation can prevent some of the long-term changes in muscle composition and fatigability. In addition, we show that regenerated axons can carry electrical signals across the injury site. Together, these studies identify muscle composition and regenerated axon excitability as post-injury features that can contribute to behavioral recovery.

Introduction

Mammalian spinal cord injuries (SCIs) can affect nearly all systems innervated at and caudal to the injury level, resulting in permanent sensory and motor deficits. Injuries that are more rostral along the spinal cord are more detrimental, while cervical injuries make up between 49.3-61.5% of all SCIs [7]. Since the first peak risk in SCI risk occurs early in life (adolescence in women and young adulthood in men) survivors will meet life-long financial, social, and physical consequences [6, 8].

After an SCI, a multitude of factors hinder the reestablishment of normal tissue histology and return of function. First, the inflammatory response causes additional tissue damage and exacerbates injury severity [3]. Studies have worked to address this secondary damage. For example, treatment with anti-inflammatory cytokine interleukin-10 (IL10) can decrease neuromuscular junction (NMJ) denervation [**Chapter 3**], apoptosis of peri-injury mature neurons, and lesion size, resulting in improved behavioral recovery [37, 85, 159, 161-166, 171]. Second, reactive astrogliosis causes the formation of a glial scar that physically prevents the

regeneration of tissues lost at the injury epicenter [187]. This physical barrier has been addressed by studies that showed scar formation can be decreased when the lesion cite is filled with a biomaterial [52, 62, 188-194]. Third, the intrinsic regenerative capacity of neurons in the central nervous system (CNS) cannot be sustained in the presence of growth inhibitory factors and absence of trophic factors in the injury microenvironment [48]. This chemical barrier to regeneration has also been addressed. The delivery of trophic factors, such as brain-derived neurotrophic factor (BDNF), can increase axonal regeneration and myelination after an SCI [34, 87, 92-95, 102]. While many methods have been explored to address inflammation, scarring, and regeneration separately, there has yet to be a study that has shown full recovery of fine motor control. A more effective therapy is needed, so perhaps a combinatorial approach may be used to address the multitude of obstacles that prevent a complete recovery.

Historically, SCI studies have focused heavily on sparing tissues from secondary damage and knocking down the barriers to regeneration. Little attention has been given to understand the remaining impediments to a full recovery, after tissues are spared and axons have been regenerated. Following an injury, muscle fibers that remain denervated for prolonged periods of time will begin to atrophy, while muscle composition will slowly shift such that the ratio of highly fatigable fibers to fatigue-resistant fibers increases [113-117, 130, 134-136]. Together, muscle mass reduction and fiber-type shifting cause decreases in contractile force and fatigue resistance [137, 138]. Though we have previously shown that lentiviral IL10 treatment can spare NMJs from denervation at 2 weeks post-injury (wpi) [**Chapter 3**], whether muscle fibers are subsequently spared from atrophy and fiber type-shifting at late timepoints remains unknown. Additionally, while our lab and many others have used BDNF to augment axonal regeneration, whether regenerated axons can carry electrical signals across an injury site also remains to be

investigated. Post-injury muscle composition and the electrophysiological properties of regenerated axons are two major factors that require further investigation, because they hold the potential to contribute to behavioral recovery at late timepoints after injury.

Therefore, these studies investigate the physiological changes and limitations that remain to hinder the full return of behavioral function after a combinatorial therapy of lentiviral IL10 and BDNF delivered via implantation of a poly(lactide-co-glycolide) (PLG) bridge into a left C5 lateral hemisection. We used lentiviral firefly luciferase (FLuc) for control injured animals, as well as sex- and age-matched naïve animals for uninjured controls. First, we hypothesized that early sparing of NMJ innervation can prevent some of the subsequent changes in muscle physiology. We examined innervation and fiber-type composition in the acromiotrapezius (ATZ) muscle. From electromyogram (EMG) recordings in response to optogenetic stimulation, we quantified muscle activatability and fatigability as signal-to-noise ratios (SNRs), peak-to-peak (P2P) amplitudes, and mean absolute values (MAVs). Then, we used two-term exponential modeling to further characterize fatigue rates with sustained muscle activation. We also hypothesized that the neuroprotective effects of IL10 in combination with the neurotrophic support of BDNF might further increase tissue sparing and augment the regenerative response. We utilized the PLG implant, which clearly delineates between intact and regenerated tissues, to isolate regenerated axons for neurofilament (NFM) quantification, filament tracing, and electrophysiological analyses.

Materials and Methods

Lentiviral Gene Delivery

Lentiviral vectors for FLuc using pLenti-CMV-Luciferase2, IL10 using pLenti-CMV-IL10, and BDNF using pLenti-CMV-BDNF were produced by transfecting HEK-293FT cells

(American Type Culture Collection, Manassas, VA) with packaging vectors in Opti-MEM (Life Technologies, Carlsbad, CA, #31985062) and Lipofectamine 2000 (Life Technologies #11668019) as previously described [37]. The virus was collected after 48hrs of incubation, precipitated using PEG-It (Systems Biosciences, Palo Alto, CA, #LV825A-1), and a total of 4E7 IFU were loaded onto a PLG scaffold [36, 37, 106]. For individual treatment conditions, a 1:1 ratio of therapeutic to FLuc virus was used. For example, the IL10 alone condition is composed of 2E7 IFU of lentiviral IL10 and 2E7 IFU of lentiviral FLuc, while the IL10+BDNF condition is composed of 2E7 IFU of lentiviral IL10 and 2E7 IFU of lentiviral BDNF. The scaffolds were produced by polymerizing PLG particles around 63-106 μm NaCl at a 1:2 by mass ratio and nine 150-250 μm diameter A-P strands of sugar that were leached to produce pores for cell infiltration and conduits to guide axon growth, respectively [5, 50].

Animals and Surgery

The Institutional Animal Care and Use Committee at the University of Michigan approved all procedures carried out on these animals. We used C57BL/6 (Jackson Laboratories, Bar Harbor, ME, #000664), Thy1-ChR2-YFP line 18 (Jackson Laboratories #007612), and CrymRFP (bred from Mutant Mouse Resource & Research Center #036627-UCD and Jackson Laboratories #007905) mice that were 2-3 months old at the time of injury. All uninjured animals are age-, sex, and genotype-matched.

Acute SCIs were performed as previously described in **Chapter 3**. Briefly, under 2% isoflurane, the surgical site was sterilized and injected with bupivacaine (0.8 mL/kg). After a C5 laminectomy, a 1 mm (A-P) left lateral hemisection was made using a microfeather microscalpel (VWR, Radnor, PA, #72045-15). The excised spinal tissue was replaced with the PLG implant, Gelfoam (Pfizer, New York, NY, #0009-0315-08) was used to cover the laminectomy site, the

overlying muscles were sutured using 5/0 Chromic Gut (Henry Schein, Melville, NY, #3101-8824), and the skin was stapled.

Histological Analyses

Histology and analyses for NMJs were carried out as previously described in **Chapter 3**. Only the injured, ipsilateral side was analyzed in reference to uninjured controls, because we had previously shown in **Chapter 3** that the uninjured, contralateral side is affected by our injury. For examining axons positive for NFM, flash frozen spinal tissues were cryosectioned at 12 μm in the transverse plane, then stained following a standard immunohistochemistry protocol with fixation in 4% paraformaldehyde. For muscle fiber type analyses, flash frozen muscles were cryosectioned at 14 μm in the transverse plane, then stained following a standard immunohistochemistry protocol without fixation. Antibodies used were chicken anti-NF200 (1:250, AVES Labs, Davis, CA #NFH) for neurofilaments, anti-bungarotoxin conjugated to Alexa Fluor 647 (1:500, Thermo Fisher, Waltham, MA #B35450) for motor endplates, rabbit anti-GAP43 (1:100, Millipore, Burlington, MA, #AB5220) for growth cones, mouse IgG1 anti-MHC IIa (1:100, Developmental Studies Hybridoma Bank (DSHB), Iowa City, IA, #SC-71) for type IIa fibers, mouse IgM anti-MHC IIb (1:100, DSHB #BF-F3) for type IIb fibers, and rabbit anti-NF200 (1:200, Sigma, St. Louis, MO, #N4142) for neurofilaments. Secondary antibodies were Alexa Fluor 488 goat anti-chicken (1:1000, Jackson ImmunoResearch, West Grove, PA, #103-547-008), Alexa Fluor 594 goat anti-rabbit (1:100, Jackson ImmunoResearch #111-587-003), Alexa Fluor 555 goat anti-mouse IgG1 (1:1000, Invitrogen, Waltham, MA, #A-21127), Alexa Fluor 647 goat anti-mouse IgM (1:1000, Invitrogen #A-21042), and Alexa Fluor 488 goat anti-rabbit (1:1000, Invitrogen #A-11070). Tissues were imaged as previously described in **Chapter 3**.

For NFM quantifications, a single observer, blinded to the experimental condition, outlined the inner wall and contents of the bridge implant as the region of interest (ROI). Then, NFM positive filaments within this ROI were quantified using a semi-automated counting program written in MATLAB as previously described [195]. A minimum of four sections were quantified for each spinal cord. For muscle fiber quantifications, two observers blinded to the experimental condition manually counted the number of MHC IIa+ and MHC IIb+ muscle fiber using the cell counter plugin in FIJI [173]. Then, the total area of the section was measured by outlining the muscle. The area of MHC IIa and MHC IIb fibers was calculated by establishing a threshold and using the measure function. A minimum of four sections was quantified for each muscle.

Tissue Clearing and Filament Analysis

Tissue clearing was achieved using a modified passive CLARITY protocol [196, 197]. Briefly, perfused tissues were further fixed in 4% paraformaldehyde, then A4P0 (4% acrylamide and 0.25% 2,2'-azobis[2-(2-imidazolin-2-yl)propane] dihydrochloride in phosphate buffered saline (PBS)) for 1 week each at 4°C. Tissues were then polymerized for 4-5 hrs at 40°C and cleared for 1 week in 8% SDS with 200 mM boric acid at pH 8.5 at 37°C. Tissues were then washed thoroughly with PBS, blocked in 6% bovine serum albumin with 0.5% Triton X-100 in PBS, stained with primary antibodies, washed with PBS, stained with secondary antibodies, and washed with PBS for two weeks each. Primary antibodies used were rabbit anti-NF200 (1:50, Sigma #N4142) for neurofilaments, mouse anti-NeuN (1:50, Millipore #MAB377) for mature neurons, chicken anti-GFAP (1:50, AVES #GFAP) for glial scarring, and rat anti-RFP (1:100, ChromoTek, Islandia, NY, #5F8) for counterstaining RFP in CrymRFP animals. Secondary antibodies used were Alexa Fluor 594 goat anti-rabbit (1:100, Jackson ImmunoResearch #111-

587-003), Alexa Fluor 647 donkey anti-mouse (1:100, Jackson ImmunoResearch #715-606-150), Alexa Fluor 488 goat anti-chicken (1:100, Jackson ImmunoResearch #103-547-008), and Alexa Fluor 594 goat anti-rat (1:100, Jackson ImmunoResearch #112-587-003). Tissues were then mounted in standard CUBIC-mount for imaging on a confocal laser scanning microscope (Olympus, Shinjuku City, Tokyo, Japan, #FV1000), using a 10x UPlanSApo lens (Olympus #1-U2B824). Images were analyzed in Imaris version 9.5.

Optogenetic Stimulation

As described in **Chapter 3**, Thy1-ChR2-YFP mice were anesthetized using 2% isoflurane, a C3-C6 laminectomy was performed, and the overlying dura was removed. An LED probe (Plexon, Dallas, TX, #OPT/FS-Flat-110/125-1L) was inserted (1 mm D-V) into the left C4. A PlexBright Controller was used to drive optical stimulation (0.04 mW) through a 465 nm HELIOS headstage (Plexon #OPT/LED_Blue_HELIOS_LC_Kit). For both baseline EMG and intraspinal recordings, we used 20 ms pulse widths at 1 Hz for a minimum of 3 minutes per animal. For muscle fatiguing, we used 50, 100, 200, 500, and 1000 ms pulse widths. Each pulse width was delivered 5 times in a row at a 2% duty cycle. For subsequent intraspinal recordings, we transected the right C5 to isolate the signals passing through the left C5 bridge implantation area and recorded for 3 minutes. We then transected the left C5, through the implant, and recorded for an additional 3 minutes to isolate noise within the system. All intraspinal recordings were taken with the initial stimulation parameters (20 ms pulse width, 1 Hz).

Data Acquisition and Processing

Dually implanted needle electrodes (Natus Neurology, Pleasanton, CA, #019-475400) were used for EMG recordings. For intraspinal recordings, we dually implanted wire electrodes (A-M Systems, Sequim, WA, #377100) into the left C6. The left ankle was used as ground.

Signals from the Plexbright Controller and implanted electrodes were sent to two different headstages (Tucker-Davis Technologies, Alchua, FL, #RA16AC), then to two separate pre-amplifiers (Tucker-Davis Technologies #RA16PA), then to a single RX7 system (Tucker-Davis Technologies) such that stimuli and recordings could be time-locked. All recordings were acquired at a synchronized rate of 24,414 Hz with bandpass frequencies of 2.2 Hz - 7.5 kHz. The difference between EMG electrode pairs was taken, then bandpassed at 100-500 Hz and analyzed using custom MATLAB® scripts.

For intraspinal recordings, males and females were combined. All other analyses considered males and females separately. SNR and P2P values were calculated as previously described in **Chapter 3**. C6 recordings for which the P2P did not decrease after subsequent transections were excluded under the assumption that the equipment shifted during the transection procedure. For analysis of fatigue, the MAV was calculated by taking the mean absolute amplitude for either the first or last 20 ms of each stimulus duration, then averaging by the number of stimulus pulses. For exponential modeling of fatigue, the absolute amplitude was average across all pulses at each stimulus duration, then smoothed using a 20 ms window to obtain a smoothed absolute amplitude (SAA) as a function of time (t), which is defined as:

$$SAA(t) = Ae^{-bt} + Ce^{-dt}, \qquad (1)$$

where A & C represent the initial maximum amplitude and b & d represent the decay constants of higher-amplitude/faster-fatigue and lower-amplitude/slower-fatigue fibers, respectively. These data were fitted using the *NonLinearLeastSquares* and *exp2* fit options. Values for which the difference between the 95% and 5% confidence interval exceeded the 50% estimate were excluded for low fitting accuracy.

Preliminary Results & Discussion

IL10 Sparing is Only Observable at Early Timepoints

We had previously shown in **Chapter 3** that lentiviral IL10 can spare NMJs from denervation after injury in the left ATZ in males and females at 2 wpi. Here, we asked how the addition of BDNF would affect the injury response and if histological differences persist over time. All four conditions (FLuc, IL10, BDNF, and IL10 + BDNF) were compared to uninjured controls as a reference point.

In the 2 wpi ATZ of females, we found that IL10 had significantly increased motor endplate and innervated NMJ densities (**Figure 12A, B**), that FLuc and BDNF conditions had significantly decreased fraction of innervated NMJs (**Figure 12C**), and that FLuc showed significantly increased reinnervation (**Figure 12D**). Importantly, examining the fraction of innervated NMJs showed that IL10 and IL10 + BDNF conditions were not significantly different from that of uninjured controls (**Figure 12C**), whereas IL10 + BDNF was the only condition that showed no difference from uninjured controls in all measures of NMJ quality (**Figure 12A-D**). Innervation differences among uninjured, FLuc, and IL10 conditions were corroborated by EMG data in both male and female mice. In the 2 wpi left ATZ, the SNR of females and the SNR and P2P of males treated with FLuc are significantly decreased relative to that of uninjured animals, whereas no differences could be found between IL10-treated and uninjured control animals (**Figure 12E-H, Chapter 3**). Preliminary histological results suggest that IL10 + BDNF spares NMJs from denervation as well as, if not better than, IL10 alone. However, to verify these histological findings, additional 2 wpi EMG data for BDNF and IL10 + BDNF (**Figure 12E-H**), which were excluded from statistical analyses due to low animal numbers, will be collected in ongoing experiments.

In the 12 wpi ATZ, we found no histological differences between our experimental conditions and the uninjured controls (**Figure 12I-L**). We also found no electrophysiological differences between FLuc and IL10 experimental conditions and the uninjured controls (**Figure 12M-P**). Additional animals are needed for 12 wpi BDNF and IL10 + BDNF EMG data, so those have been excluded from the statistical analyses (**Figure 12M-P**). Since the early NMJ sparing effects of IL10 and IL10 + BDNF from 2 wpi can no longer be observed at 12 wpi, likely because of disintegration of denervated motor endplates and muscle atrophy, these preliminary results suggest that NMJ innervation is not a major contributor to the behavioral deficits that remain at late timepoints after an SCI (**Chapter 3**). All p-values are reported in **Table 3**.

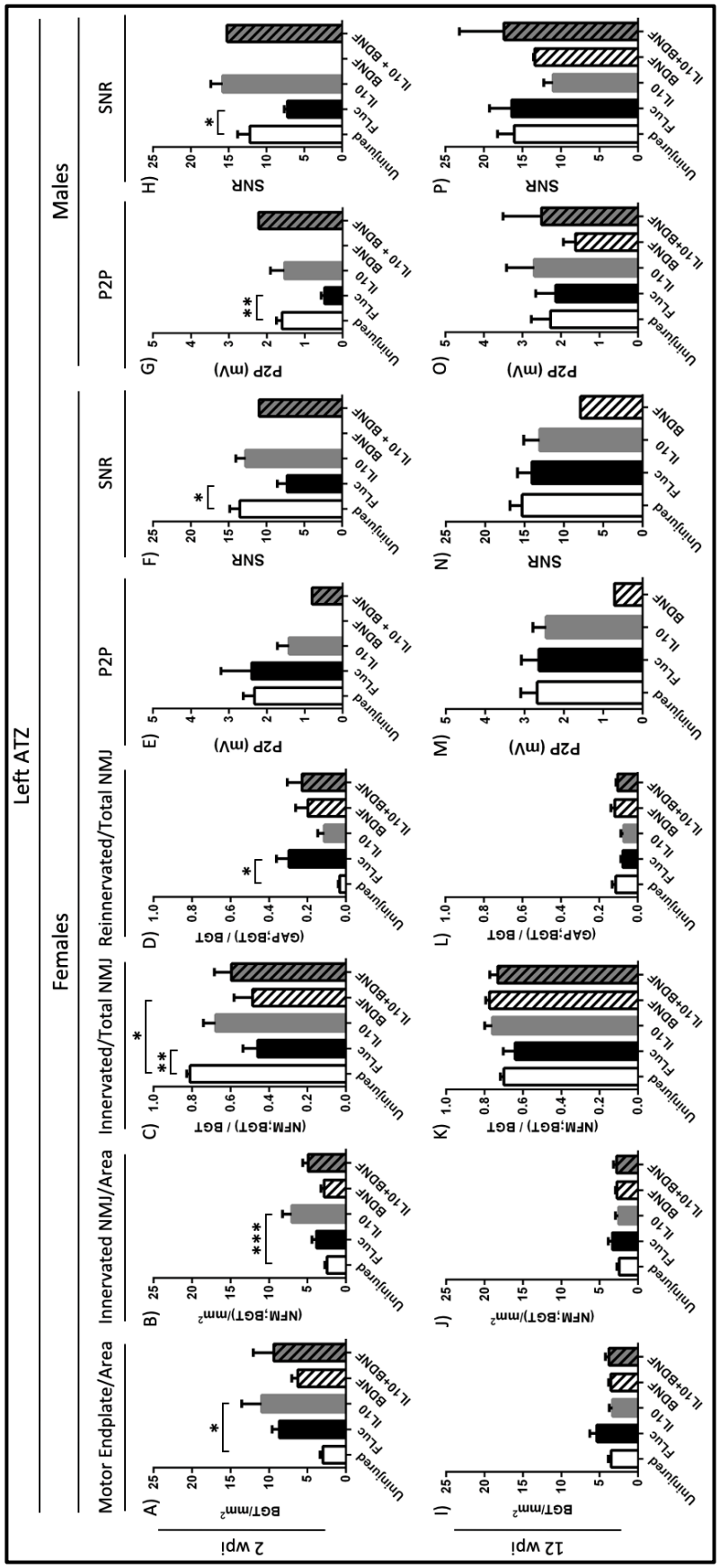

Figure 12. Quantifications of motor endplate density normalized to muscle area (A, I), innervated NMJ density normalized to muscle area (B, J), fraction of total motor endplates that are innervated (C, K), and fraction of total motor endplates that are being reinnervated (D, L) are shown for 2 wpi (A-D) and 12 wpi (I-L) females. n = 5 - 6 animals/condition. The P2P (E, G, M, O) and SNR (F, H, N, P) for 2 wpi (E, F) and 12 wpi (M, N) females, and for 2 wpi (G, H) and 12 wpi (O, P) males were quantified as well. 2 wpi Uninjured, FLuc, and IL10 data are taken from ***Chapter 3****. n = 4 - 8 animals/condition, except BDNF (n = 1 for 12 wpi females, n = 2 for 12 wpi males) and IL10 + BDNF (n = 1 for 2 wpi females, n = 1 for 2 wpi males, n = 0 for 12 wpi females, n = 3 for 12 wpi males). Error bars are ± SEM. One-Way ANOVA with Dunnett's Post-Hoc *p < 0.05, **p < 0.01, ***p < 0.001. Note: BDNF and IL10+BDNF conditions were excluded from statistical analyses in panels E-H and M-P.*

Figure #	One-Way ANOVA p-Value	Dunnett's Post-Hoc p-value			
		Uninjured vs. FLuc	Uninjured vs. IL10	Uninjured vs. BDNF	Uninjured vs. IL10 + BDNF
12A	0.0327	0.0789	0.0134	0.4943	0.0535
12B	0.0013	0.4256	0.0007	0.9832	0.0780
12C	0.0179	0.0091	0.5544	0.0215	0.1722
12D	0.0274	0.0100	0.7357	0.1672	0.0831
12E	0.2207	0.9886	0.2068	N/A	N/A
12F	0.0207	0.0139	0.8723	N/A	N/A
12G	0.0052	0.0047	0.9686	N/A	N/A
12H	0.0045	0.0451	0.1561	N/A	N/A
12I	0.0959	0.0957	0.9989	> 0.9999	0.9880
12J	0.5710	0.3633	0.9992	0.9602	0.9302
12K	0.1712	0.7242	0.7147	0.5218	0.9470
12L	0.1370	0.3034	0.2377	0.9963	0.9801
12M	0.9213	0.9964	0.8934	N/A	N/A
12N	0.6635	0.8507	0.5742	N/A	N/A
12O	0.7965	0.9757	0.8349	N/A	N/A
12P	0.3094	0.9910	0.3141	N/A	N/A

*Table 3. One-Way ANOVA p-values and Dunnett's Post-Hoc p-values associated with **Figure 12**..*

Injury Affects Muscle Composition and Fatigability

Since muscle atrophy and changes in muscle fiber types that compose a muscle occur after an SCI, we wanted to see if early NMJ sparing could prevent changes in muscle composition, activation, and fatigability at late timepoints. Histological analysis is in progress for Type IIa and IIb fibers in the left ATZ at 2 and 12 wpi (**Figure 13**).

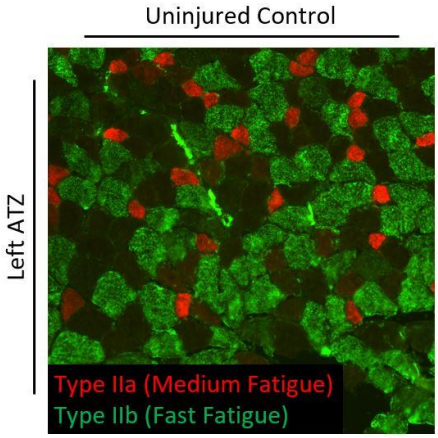

Figure 13. Histology of the left ATZ of an uninjured control mouse stained for Type IIa (red) and Type IIb (green) fibers. Quantifications for 2 and 12 wpi tissues are in progress.

Next, we took EMG recordings at 2 and 12 wpi using successively longer optogenetic stimulation durations. We examined the first 20 ms of the stimulus, also known as the initial

MAV, and the last 20 ms of the stimulus, also known as the sustained MAV. Comparisons were first done between conditions, to identify any differences in activation due to treatment at each timepoint. Comparisons were also done between 2 and 12 wpi, to check whether differences within each condition are due to changes in the muscle over time.

In 12 wpi females, preliminary results comparing different treatments show that FLuc-treated animals had a significantly increased initial MAV when compared to control uninjured animals for 200, 500, and 1000 ms stimulation durations (**Figure 14C**). Since these differences were not observable when muscles were given only short stimulus durations (**Figure 12M, N**), these results suggest FLuc-treated females experienced increased recruitment of fast-fatigue muscle fibers with increased muscle activation. Meanwhile, 12 wpi IL10-treated animals exhibited no difference in initial MAV from that of uninjured control animals, suggesting IL10 is able to prevent some of the long-term changes in muscle activation that FLuc-treated animals experienced. In 12 wpi males, IL10 significantly increased the sustained MAV when compared to control uninjured animals for 50, 100, 200, and 500 ms stimulation durations (**Figure 14H**), suggesting an increase in motor unit size for fatigue-resistant fibers. No other differences were found across the rest of the female (**Figure 14A-D**) or male (**Figure 14E-H**) conditions. Ongoing studies will aim to add more animals to this analysis for better data resolution. All p-values associated with **Figure 14A-H** are reported in **Table 4**.

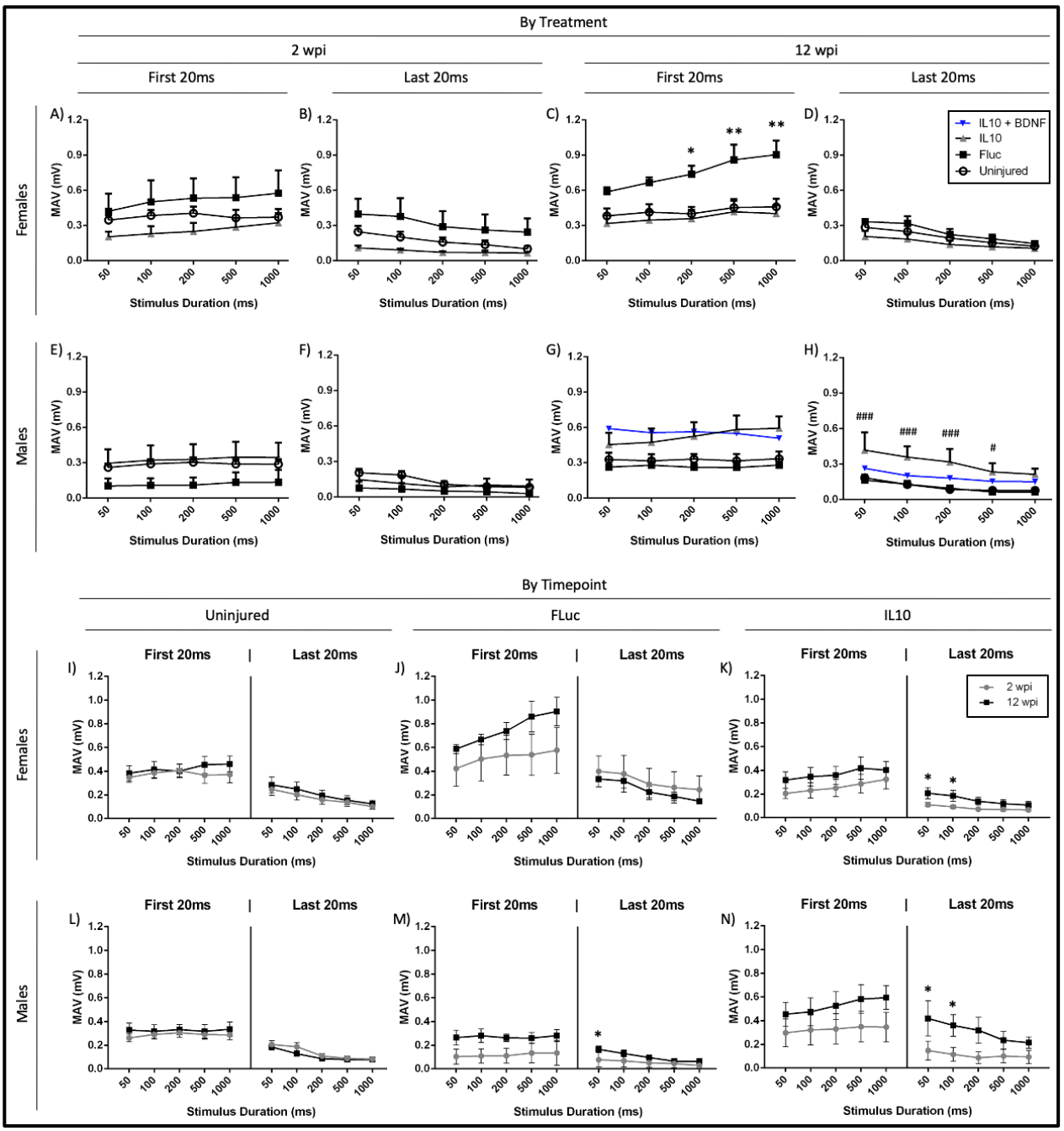

*Figure 14. Quantification of MAV for the first 20 ms (A, C, E, G) and the last 20 ms (B, D, F, H) of different stimulus durations for females (A-D) and males (E-H) at 2 wpi (A, B, E, F) and 12 wpi (C, D, G, H). Error bars are ± SEM. Two-Way Repeated Measures ANOVA with Dunnett's Post-Hoc *p < 0.05, **p < 0.01 for uninjured vs. FLuc, while $^{\#}p < 0.05$, $^{\#\#}p < 0.01$, $^{\#\#\#}p < 0.001$ for uninjured vs. IL10. Quantification of MAV for female (I, J, K) and male (L, M, N) uninjured controls (I, L), FLuc (J, M), and IL10 (K, N) treatment for comparison of 2 and 12 wpi. Error bars are ± SEM. Multiple t-test *p < 0.05. n = 3 - 10 animals/condition, except FLuc (n = 2 for 2 wpi males) and IL10 + BDNF (n = 1 for 12 wpi males). Note: IL10+BDNF condition was excluded from statistical analyses in all panels.*

Figure #	Two-Way Repeated Measures ANOVA p-value			Dunnett's Post-Hoc p-value									
				Uninjured vs. FLuc					Uninjured vs. IL10				
	Inter -action	Stimulus Duration	Treat -ment	50 ms	100 ms	200 ms	500 ms	1000 ms	50 ms	100 ms	200 ms	500 ms	1000 ms
14A	0.1975	0.0014	0.2210	0.7778	0.5602	0.5016	0.3025	0.1942	0.3671	0.3056	0.3042	0.7170	0.8853
14B	0.2284	<0.0001	0.0793	0.1503	0.0868	0.2303	0.2624	0.1901	0.1551	0.2813	0.4454	0.6054	0.8540
14C	0.0040	<0.0001	0.0305	0.1871	0.0874	0.0167	0.0035	0.0014	0.7889	0.7759	0.9047	0.9302	0.8297
14D	0.8665	<0.0001	0.6265	0.7985	0.6519	0.9157	0.9025	0.9559	0.5083	0.6260	0.7082	0.8669	0.9611
14E	0.9508	0.2091	0.2487	0.2735	0.1817	0.1511	0.2779	0.2931	0.8994	0.9280	0.9530	0.7614	0.7657
14F	0.0588	<0.0001	0.3809	0.0683	0.0980	0.5273	0.6965	0.5763	0.4275	0.2853	0.8743	0.9612	0.9666
14G	0.1257	0.0860	0.0726	0.7049	0.8832	0.6615	0.7566	0.7777	0.3454	0.2067	0.1026	0.0197	0.0234
14H	0.1297	<0.0001	0.0108	0.9111	0.9988	0.9801	0.9614	0.9552	0.0008	0.0009	0.0008	0.0271	0.0595

*Table 4. Two-Way Repeated Measures ANOVA p-values and Dunnett's Post-Hoc p-values associated with **Figure 14A-H**. Note: p < 0.0001 for subject matching in all panels.*

Next, comparing early and late timepoints, both female and male control uninjured animals showed no differences for both initial and sustained MAV (**Figure 14I, L**), suggesting 10 weeks of ageing had little effect on muscle activation. In FLuc-treated males, the sustained MAV for 50 ms stimulus duration was significantly higher at 12 wpi when compared to 2 wpi (**Figure 14M**). In IL10-treated females and males, the sustained MAVs for 50 and 100 ms stimulus durations were significantly higher at 12 wpi when compared to 2 wpi (**Figure 14K, N**). No differences could be observed for FLuc-treated females (**Figure 14J**). Together, these preliminary results suggest injury changes how muscles are activated as an animal ages, though more animals are needed to confirm these findings. All p-values associated with **Figure 14I-N** are reported in **Table 5**.

Figure #	Multiple T-Test p-value									
	First 20 ms					Last 20 ms				
	50 ms	100 ms	200 ms	500 ms	1000 ms	50 ms	100 ms	200 ms	500 ms	1000 ms
14I	0.6895	0.7529	0.9539	0.3298	0.3240	0.5633	0.4760	0.5994	0.8035	0.7277
14J	0.4109	0.4147	0.3097	0.1162	0.1109	0.6454	0.6700	0.6356	0.5902	0.4954
14K	0.2867	0.2715	0.3045	0.2162	0.4548	0.0251	0.0303	0.1164	0.2454	0.3180
14L	0.3152	0.6974	0.6868	0.6877	0.4752	0.5165	0.0680	0.4752	0.7545	0.8876
14M	0.0898	0.0714	0.1091	0.1772	0.1200	0.0376	0.1350	0.2721	0.6168	0.3829
14N	0.3576	0.3717	0.2551	0.1797	0.1551	0.0308	0.0489	0.0610	0.2654	0.3177

*Table 5. Multiple t-test p-values associated with **Figure 14I-N**.*

While analysis of the initial and sustained MAV provides innervation and activation insight for fast-fatigue and fatigue-resistant fibers, we sought a more informative way to understand how muscle activation changes within a stimulus duration. We noticed that long stimulus durations produced EMG signals that exhibited exponential decay characteristics, so we applied two-term exponential modeling using equation (1), which would capture the initial amplitude of both fast-fatigue and fatigue-resistant fibers and their individual rates of decay. A graphical example of this analysis can be seen in **Figure 15**. When more animals become available for analysis, the constant values will be compared across treatment conditions and timepoints. We hypothesize that injury increases the decay rates of both fast-fatigue and fatigue-resistant fibers, while tissue sparing due to IL10 can prevent some of the injury-induced increases in fatigability.

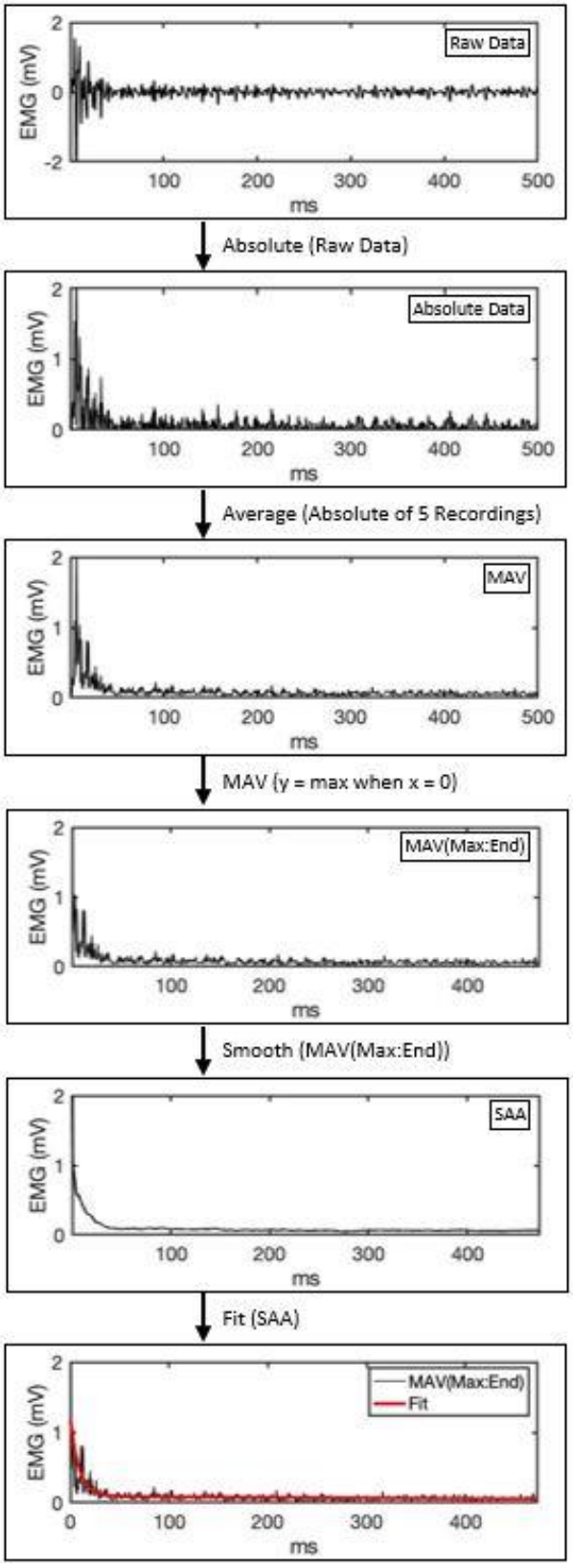

Figure 15. Graphical representation of exponential modeling applied to the EMG recording of the left ATZ in an uninjured female that is receiving optogenetic stimulation in the left C4.

Gene Therapy Enhances Axon Regeneration Across an SCI

Next, we moved to examine how different virus conditions can influence axonal regeneration by quantifying NFM within the bridge. We found that 2 wpi animals treated with either IL10 or IL10+BDNF had significantly greater NFM densities than FLuc-treated animals, and that animals treated with IL10+BDNF had a significantly greater NFM density than animals treated with BDNF alone (**Figure 16B**). However, these differences could no longer be observed by 12 wpi (**Figure 16C**). Together, these results suggest that decreased inflammation enhances the onset of regeneration, but not necessarily the total regenerative capacity as long as a PLG implant is present.

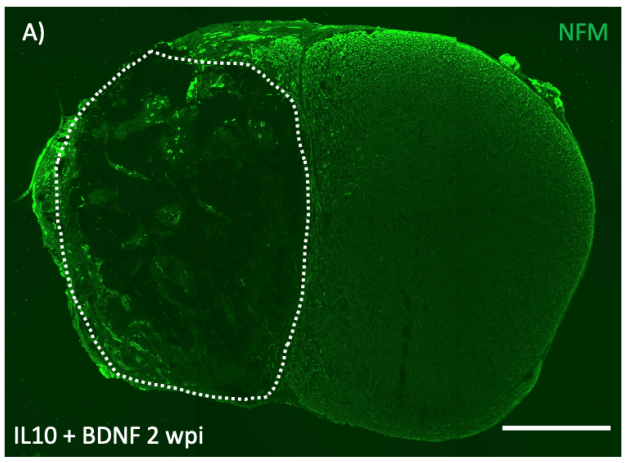

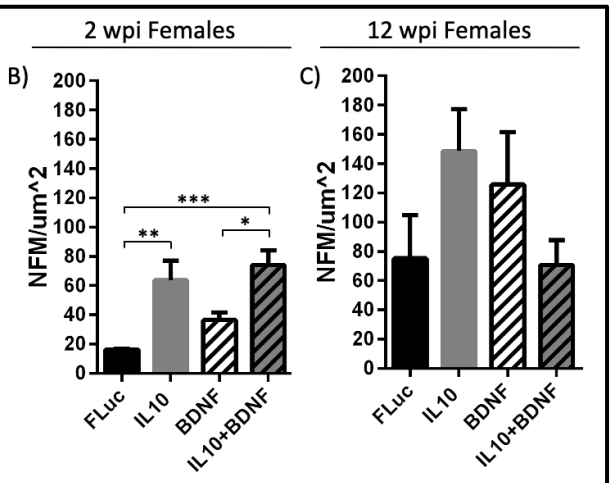

Figure #	One-Way ANOVA p-Value	Tukey Post-Hoc p-value					
		FLuc vs. IL10	FLuc vs. BDNF	FLuc vs. IL10 + BDNF	IL10 vs. BDNF	IL10 vs. IL10 + BDNF	BDNF vs. IL10 + BDNF
16B	0.0007	0.0078	0.3718	0.0009	0.1551	0.8385	0.0232
16C	0.2214	0.3502	0.6188	0.9995	0.9435	0.2988	0.5494

*Figure 16. Representative images of spinal cords (A) stained for NFM. Quantifications of neurofilament normalized to bridge area for 2 (B) and 12 (C) wpi females. n = 5 - 6 animals/condition. Error bars are ± SEM. One-Way ANOVA with Tukey Post-Hoc *p < 0.05, **p < 0.01, **p < 0.001. Scale bar = 500 μm.*

Since there exists no synaptic targets within the bridge, we then asked whether these axons are traversing the entire injury site. In a hemisection model, where intact, contralateral tissues have the potential for axon sprouting, plasticity, and appearance caudal to the injury, 3D tracing studies can provide much greater anatomical insight than 2D slice histology. Using

CLARITY in a wild type, FLuc-treated 26 wpi animal, we found that NFM positive, regenerated axons can easily be observed within the injury site (**Figure 17A and A'**). Filament analysis shows some regenerated axons could even be traced from the rostral to the caudal end of the injury (**Figure 17A''**). However, more animals will be needed to confirm these findings.

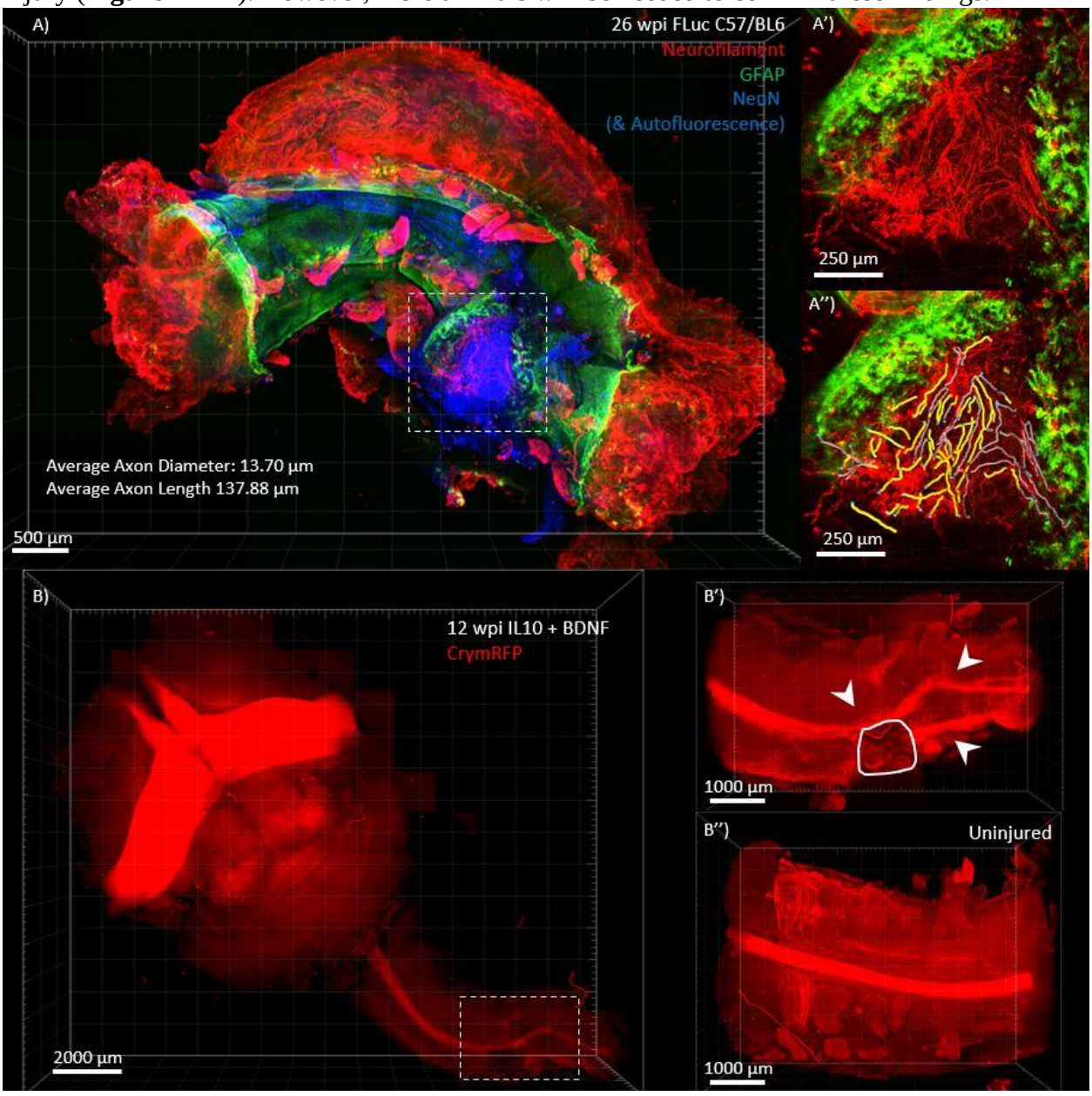

Figure 17. CLARITY images of a 26 wpi spinal cord of a wild type animal that received FLuc treatment (A) and a 12 wpi CrymRFP animal that received IL10 + BDNF. At 26 wpi, NFM positive axons can be observed in abundance throughout the injury site, which is outlined in a dotted box and a magnified view is shown (A'). Filament tracing (A'') was able to be carried out on NFM positive axons and the average diameter and length of traceable axons are indicated. At 12 wpi, CrymRFP positive axons were not traceable throughout the injury or peri-injury tissues, which are outlined in a dotted box and a magnified view is shown (B'). An uninjured CrymRFP positive spinal cord is shown for reference (B''). Arrowheads point towards axon bundles and the solid white box outlines the implant area.

Next, since fine motor control is most relevant to human behavior, we looked more specifically in CrymRFP animals, whose corticospinal tract (CST) axons carry a fluorescent tag. The 12 wpi IL10+BDNF-treated CrymRFP spinal cord (**Figure 17B and B'**) that we analyzed appeared to have its one CST axon bundle on the rostral end of the injury split into one medial bundle and one lateral bundle at the caudal end of the injury. This is an abnormal finding in comparison to uninjured CrymRFP tissues (**Figure 17B''**), which displays a single medial CST bundle along the length of the cord. However, sparse labeling within the injury prevented us from applying filament tracing to confirm if these axons grew from C4 to C6 or if they sprouted from the contralateral C5/6. While previous studies using 2D slice histology showed punctate staining for CST axons within the injury site [104], higher quality images and more animals for our 3D tracing studies will be needed to confirm that CST axons can regenerate across an SCI. Furthermore, due to the medial location of the CST, a full transection model might provide a cleaner analysis of CST regeneration.

Regenerated Axons Are Electrically Active

Finally, we wanted to know if regenerated axons in the central nervous system can carry electrical signals. With optogenetic stimulation in the left C4 of cortical layer V projection neurons that express a channelrhodopsin, we took intraspinal recordings of the left C6 at 12 wpi. We transected the right C5 to isolate signals only to those traveling through the bridge in the left C5, then normalized all values to recordings in which there was a full C5 transection to account for any electrical noise emitted by the stimulating equipment. A schematic can be seen in **Figure 18A** and a sample recording can be seen in **Figure 18B**. Preliminary quantifications of signals traveling through the left C4 can be seen in **Figure 18C**. Although no statistically significant differences can be observed between conditions, since more animals are needed, we find that the

left C6 presents recordable electrical signals in almost all animals analyzed. While these preliminary results suggest that regenerated axons are electrically active, whether they form mature synapses and the identity of their synaptic targets remains to be determined in future experiments.

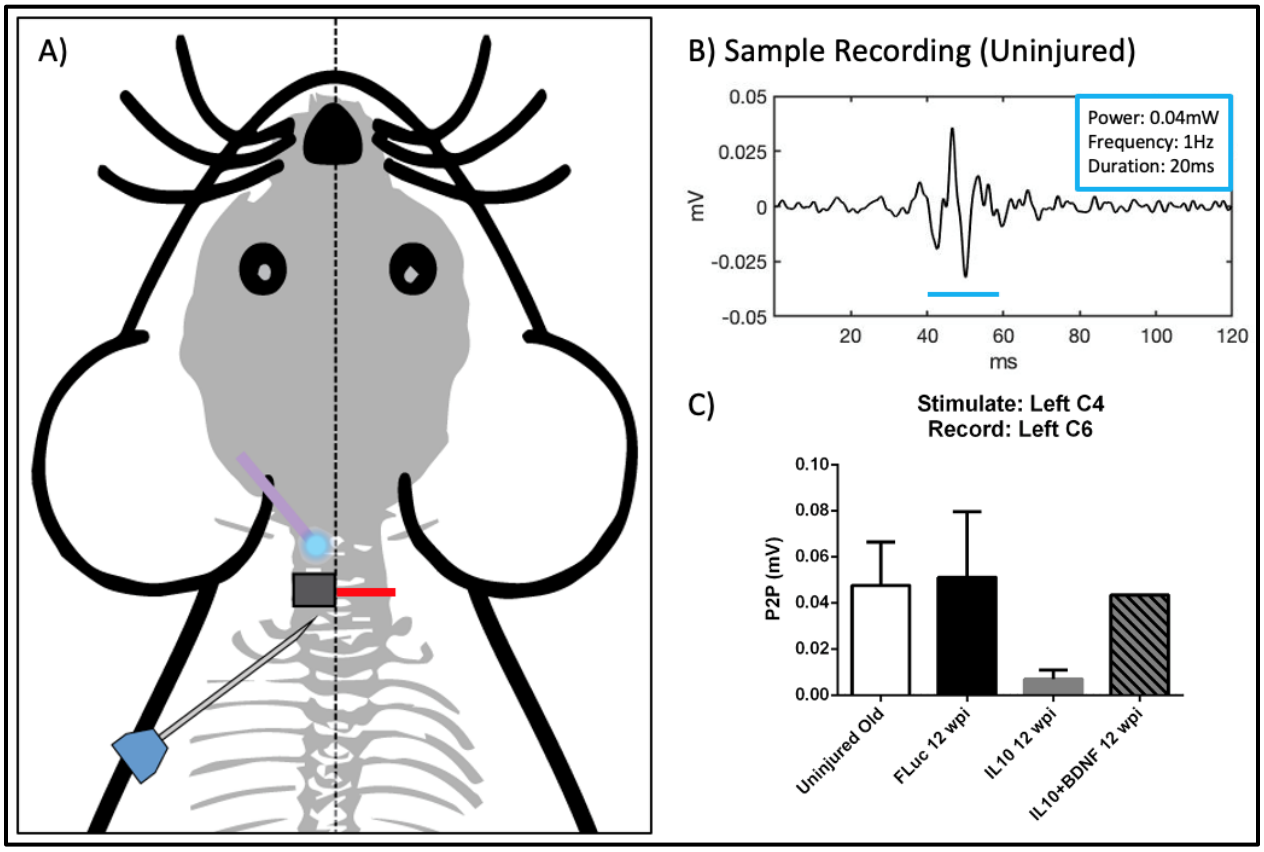

Figure 18. Schematic for intraspinal stimulation at C4 and recording at C6 (A), as well as the stimulus parameters (20 ms pulses, 0.04 mW, 3 min, 1 Hz), representative recording of an uninjured female (B), and peak-to-peak (C) quantification. n = 4 - 8 animals/condition, except for IL10 + BDNF (n = 1). Error bars are ± SEM. One-Way ANOVA with Tukey Post-Hoc.

Chapter 5 Conclusions and Future Directions

Summary of Findings

Collectively, the work described in this dissertation focuses on the histological and electrophysiological outcomes associated with the use of lentivirus-loaded PLG scaffolds to bridge a cervical SCI. The SCI is a left-sided C5 hemisection, which results in motor deficits of the left arm. At 2 and 12 wpi, we found that animals receiving anti-inflammatory IL10 lentiviral treatment exhibited greater control of their left forearm than animals who received a control lentiviral treatment. We determined that IL10 exerts its therapeutic benefits through the preservation of motor circuitry from secondary damage due to inflammation, thus allowing for more normal muscle activation characteristics. We find that this tissue sparing at early timepoints after an injury can affect how muscles atrophy and age, thus ultimately affecting the ability of the muscle to resist fatigue. Additionally, we show that regenerated axons can carry electrical signals across an injury site, thereby suggesting these axons have the potential to contribute to behavioral recovery long after an injury has occurred. The research presented here advances our understanding of the short and long-term effects of lentiviral gene therapy treatment on motor circuit integrity, muscle fatigability, and regenerated axon excitability.

Significance and Impact of Findings

Of the thousands of new SCI patients each year, most of the affected individuals will be male [1], most of the injuries will be at a cervical level [7], and none will receive acute treatment designed specifically to address the secondary damage that will contribute to their functional

deficits. While studies have identified sex-specific differences in the immune response [168-170], most SCI studies use female rodents [85, 160-164, 166, 167], and most of these are carried out at the thoracic level [85, 161-166]. In **Chapter 3**, we address the dire need for understanding how an anti-inflammatory gene therapy works in both male and female mice at an SCI level that is relevant to human motor function. We show that lentiviral IL10 has therapeutic benefits in both sexes by preventing the denervation of skeletal muscles whose LMNs reside rostral to and at our C5 hemisection. These findings demonstrate the non-sex-specific effectiveness of anti-inflammatory lentiviral IL10 for the prevention of secondary damage and amelioration of behavioral deficits in a cervical injury model.

While prevention of secondary damage substantially improves outcomes of an SCI by various measures, additional improvements remain to be made. Although animals that received IL10 treatment perform better than those who received control treatment, neither group of animals showed continued improvement between 2 and 12 wpi. Disruptions to the spinal circuitry including neuronal apoptosis, axonal degeneration, and synaptic rewiring are unavoidable in cases of traumatic SCIs. The loss of these tissues corresponds to the loss of information transfer across an injury site. In **Chapter 4**, we explored how an animal's physiology changes far after an SCI despite early anti-inflammatory gene therapy, looked to enhance the regenerative capacity by implementing a combinatorial therapy using IL10 with BDNF, and examined anatomical and electrophysiological properties of regenerated axons. Preliminary results suggest that, while muscle innervation returns to pre-injury levels by 12 wpi, differences in muscle composition and fatigability ensue. Furthermore, initial tissue sparing and the neurotrophic benefits of IL10 alone appear to have the greatest positive impact on NMJ innervation and NFM regeneration through the injury, such that the addition of BDNF is non-

additive. Finally, and importantly, we show that regenerated axons can not only be traced through the injury site, but they can also carry electrical signals. These findings highlight changes in muscle composition as a potential therapeutic target and demonstrate the ability of regenerated axons to reestablish lost circuitry.

Future Directions

Sex-specific Optimization of Anti-inflammatory Treatment

While we show in **Chapter 3** that lentiviral IL10 can spare tissues from secondary damage in both male and female mice, sex-specific differences were identified. Since previous research suggest female rodents recover significantly better than male rodents after an SCI [183, 184], we suspect that the differential outcomes seen in **Chapter 3** represent differences in the initial response to injury and not the response to IL10 treatment. These differences suggest room for optimization exists, especially during the first 2-3 days after an injury during which lentiviral expression is ramping up from subtherapeutic levels. Here, we propose a couple of options moving forward.

First, interleukin-33 (IL33) is another anti-inflammatory cytokine that reduces secondary damage and improves functional recovery in female mice [198]. A head-to-head comparison in the same injury model in both sexes will be necessary to identify which interleukin is more effective, in addition to a combined test to determine if any synergistic effects exist. Second, an alternative IL10 delivery method, such as absorption onto the implanted scaffold, may be necessary to bridge the gap in lentiviral expression during the first couple of days after an injury. Finally, since outcomes in SCI are negatively affected by the presence of testosterone [184], its reduction may ameliorate injury severity in males. A localized approach will be necessary to avoid the well-known symptoms associated with systemic testosterone withdrawal in men.

Coincidentally, testosterone is the precursor to estrogen, which has well-known neuroprotective effects after an SCI [199]. Thus, local expression of aromatase, the enzyme that is responsible for the conversion of testosterone to estrogen, may be used to dampen testosterone's detrimental effects while simultaneously taking advantage of estrogen's neuroprotective effects.

Examining Synaptic Targets of Regenerated Axons

Although in **Chapter 4** we show that regenerated axons can carry electrical signals across the injury site, that signal needs to be received by the correct target neuron for the appropriate behavioral output to occur. Axonal regeneration alone is insufficient for circuit reformation, so a series of steps are needed to achieve the accurate reconstruction of spinal circuits that are lost to an injury.

First, the ability of a regenerating axon to form a synapse is yet to be determined. Research has identified a voltage-gated calcium channel subunit that acts as a switch between axon elongation and synapse formation, which cannot occur simultaneously in a single neuron [200]. Therefore, studies are needed to determine if post-SCI regenerating axons are capable of synaptogenesis or if an additional therapeutic cue is necessary to activate this molecular switch. Second, synapse maturation does not necessarily follow synapse formation. Regenerated synapses can lack certain molecular components that are vital to their function and prevent adequate information transfer [201]. Therefore, studies are needed to determine if synapses formed by regenerated axons are functional or if an additional therapeutic cue is necessary to induce synapse maturation. Third, the synaptic target of a regenerated axon needs to be specific. Synkinesis is a symptom in which voluntary activation of a specific muscle simultaneously activates another muscle inappropriately, due to aberrant innervation patterns that commonly occur after nerve trauma. Therefore, studies are needed to determine if the synaptic targets of

regenerated axons are correct or if a combination of guided synaptogenesis and synaptic pruning are necessary to refine circuit specificity.

While histology, electrophysiology, and transsynaptic tracing are just a few techniques that may be employed to further our biological understanding, the path to reconstruct a spinal cord is not as clear. The elegance and complexity with which the nervous system is built necessitates a combinatorial approach. Only then may an affected individual step across the multitude of barriers that contribute to paralysis after an SCI.

Appendix

Temporal Control of Lentiviral Gene Expression

Authors

Longshun Li, Jessica Y. Chen, Joseph T. Decker, Lonnie D. Shea

Introduction

Although previous studies in our lab show that lentiviral gene delivery through PLG bridge implantation for IL10 is able to reduce inflammation and improve locomotor function [37, 159, 171], the long-term overexpression of lentiviral factors may have some detrimental effects. For example, persistent IL10 expression can exacerbate inflammation and cause demyelination of the sciatic nerve [202], while transgene overexpression using a strong constitutive promotor in general can decrease cell proliferation and have cytotoxic effects [203]. Therefore, inducible systems for regulating transgene expression have emerged as a means to improve the safety and efficacy of gene therapy [204, 205]. One example is the tetracycline-inducible transgenic system, in which transcription can be modulated by the introduction and withdrawal of doxycycline (DOX). Herein, we investigated the quality of an all-in-one tetracycline-inducible (TET-ON) system under HEK-293T cells, by comparing the fold change of a luciferase transgene with a constitutive promotor (CMV).

Materials and Methods

The DNA sequence for firefly luciferase (FLuc) was cloned into a pLIX_403 backbone (Addgene, Watertown, MA, #41395), and the resulting plasmid sequence confirmed via Sanger

Sequencing to produce pLIX_403-Fluc, which carried a puromycin selection sequence. The CMV-FLuc used was produced as previously described in **Chapter 3**. Both pLIX-403-Fluc and CMV-FLuc lentiviruses were produced as previously described in **Chapter 3**. HEK-293T cells were treated with either lentivirus at a cell to virus ratio of 1:10 for 24 hours, after which the cell culture media was refreshed, and the cells were allowed to recover for one day. Then the cells were treated with 10ug/ml of puromycin, which was removed after an additional 24 hours. After 14 days of recovery, the cells were passaged into a 96-well cell-culture plate in triplicates for bioluminescence imaging under an *in Vivo* Imaging System (Perkin Elmer, #124262). On day 0 (1 day after passaging), cells were either exposed to 1ug/ml of DOX or left untreated overnight. The next day, luciferin (1:100, Perkin Elmer, #122799) was added, and imaging took place 10 minutes later. This induction procedure was repeated for 3 consecutive days.

Preliminary Results

We found that the addition of DOX to cells transduced with pLIX_403-Fluc caused a significant increase in luciferase expression as described by fold change on days 1, 2, 3, and 4 (**Figure 19**). This indicates that expression can be turned on in the presence of DOX. Importantly, the absolute photon flux of pLIX_403-Fluc was not significantly different from that of CMV-FLuc (**Figure 19**), suggesting our all-in-one plasmid has the potential for transgene expression at therapeutic levels. In future experiments, we plan to culture the cells for longer such that we can withdraw DOX from the experiment while continuing the imaging, which will allow us to confirm that transgene expression is able to return to baseline after induction. One limitation of this all-in-one system is that transduction efficiency is relatively low, which became apparent when we applied puromycin and few cells survived the selection. Work may need to be done to increase our transduction efficiency, because cell selection is not feasible if we are

transducing cells *in vivo* for gene therapy. We suspect that the large size of pLIX_403-Fluc may be a major limiting factor, because increasing plasmid size has been shown to greatly reduce transduction efficiency [206]. Alternatively, we are starting a collaboration with University of Buffalo's Dr. Stelios Andreadis, who has a similar tetracycline-inducible lentiviral vector with which we can run parallel experiments using our pLIX_403-Fluc to compare efficiency and expression. Nonetheless, our preliminary results support the use of the TET-ON all-in-one system for modulating gene therapy *in vivo*.

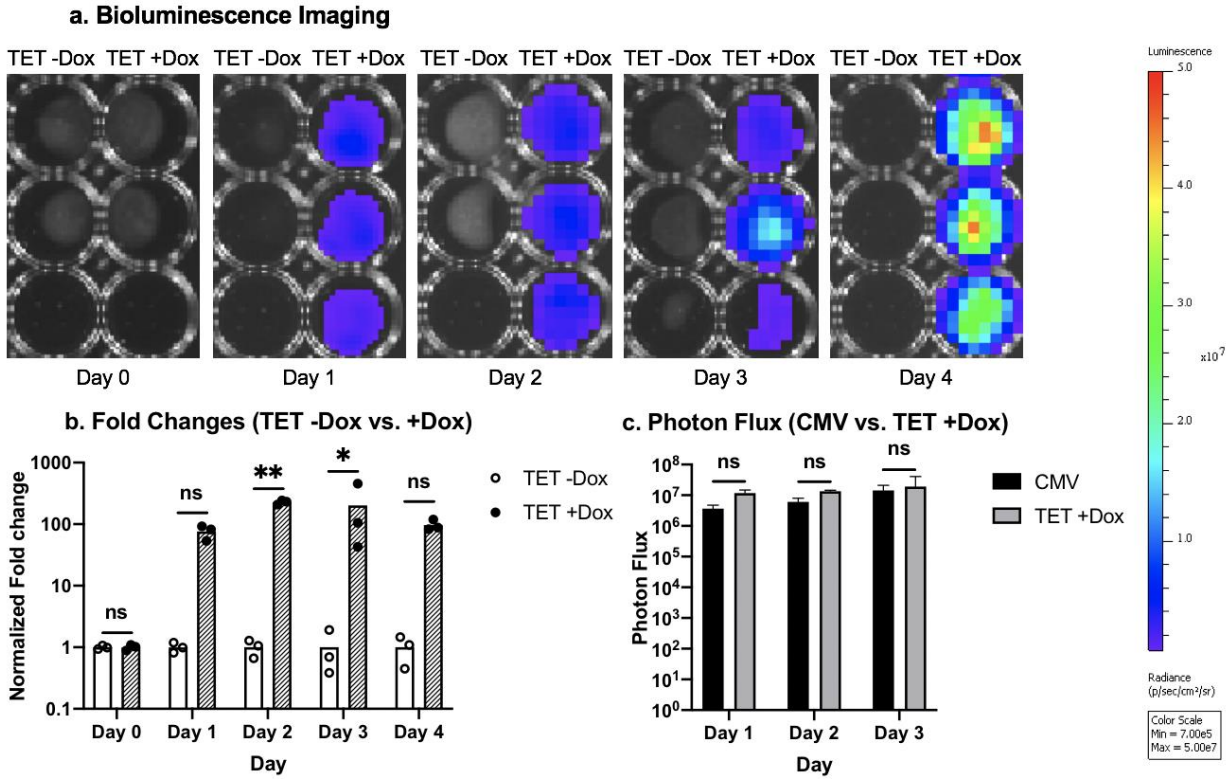

*Figure 19. IVIS Quantification of Luciferase Expression. Snapshots of bioluminescence imaging (a), normalized fold changes between TET +Dox and TET -Dox (b), and absolute photon flux comparison between CMV and TET +Dox (c). Two-way ANOVA with Tukey's post hoc test, *p<0.05, **p<0.01.*

Bibliography

1. National Spinal Cord Injury Statistics Center, U.o.A., Birmingham, *Spinal Cord Injury: Facts and Figures at a Glance.* 2019.
2. Merritt, C.H., et al., *Economic impact of traumatic spinal cord injuries in the United States.* Neuroimmunology & Neuroinflammation, 2019. **6**(9).
3. Zhang, N., et al., *Inflammation & apoptosis in spinal cord injury.* The Indian journal of medical research, 2012. **135** (3): p. 287-296.
4. Vajn, K., et al., *Axonal regeneration after spinal cord injury in zebrafish and mammals: differences, similarities, translation.* Neuroscience Bulletin, 2013. **29**(4): p. 402–410.
5. Thomas, A.M. and L.D. Shea, *Polysaccharide-modified scaffolds for controlled lentivirus delivery in vitro and after spinal cord injury.* Journal of Controlled Release, 2013. **170**(3): p. 421-429.
6. Organization, W.H., *Spinal Cord Injury.* 2013.
7. Singh, A., et al., *Global prevalence and incidence of traumatic spinal cord injury.* Clinical Epidemiology, 2014. **6**: p. 309-331.
8. Anderson, K.D., *Targeting recovery: priorities of the spinal cord-injured population.* Journal of Neurotrauma, 2004. **21**(10): p. 1371-1383.
9. Scivoletto, G., et al., *Who is going to walk? A review of the factors influencing walking recovery after spinal cord injury.* Frontiers in Human Neuroscience, 2014. **8**(141).
10. Rice, T., et al., *Characterization of the early neuroinflammation after spinal cord injury in mice.* Journal of Neuropathology and Experimental Neurology, 2007. **66**(3): p. 184-195.
11. Pineau, I. and S. Lacroix, *Endogenous signals initiating inflammation in the injured nervous system.* Glia, 2008. **57**(4): p. 351-361.
12. Bartholdi, D. and M.E. Schwab, *Expression of pro- inflammatory cytokine and chemokine mRNA upon experi- mental spinal cord injury in mouse: an in situ hybridization study.* European Journal of Neuroscience, 1997. **9**(7): p. 1422-1438.
13. Yang, L., et al., *Early expression and cellular localization of proinflammatory cytokines inter- leukin-1beta, interleukin-6, and tumor necrosis factor-alpha in human traumatic spinal cord injury.* Spine, 2004. **29**(9): p. 966-971.
14. Ley, K., *M1 means kill; m2 means heal.* Journal of Immunology, 2017. **199**(7): p. 2191-2193.
15. Anwar, M.A., T.S. Al Shehabi, and A.H. Eid, *Inflammogenesis of Secondary Spinal Cord Injury.* Frontiers in Cellular Neuroscience, 2016. **10**(98).
16. Alizadeh, A., S.M. Dyck, and S. Karimi-Abdolrezaee, *Traumatic Spinal Cord Injury: An Overview of Pathophysiology, Models and Acute Injury Mechanisms.* Frontiers in Neurology, 2019. **10**(282).
17. Gonzalez, R., et al., *Reducing inflammation decreases secondary degeneration and functional deficit after spinal cord injury.* Experimental Neurology, 2003. **184**(1): p. 456-463.

18. Bowers, C.A., B. Kundu, and G.W. Hawryluk, *Methylprednisolone for acute spinal cord injury: an increasingly philosophical debate.* Neural Regeneration Research, 2016. **11**(6): p. 822-885.
19. Lee, H.-C., et al., *Pitfalls in treatment of acute cervical spinal cord injury using high-dose methylprednisolone: a retrospect audit of 111 patients.* Surgical Neurology, 2007. **68**: p. S1:37-S1:42.
20. Short, D., W. El Masry, and P. Jones, *High dose methylprednisolone in the management of acute spinal cord injury—a systematic review from a clinical perspective.* Spinal Cord, 2000. **38**(5): p. 273-286.
21. Suberviola, B., et al., *Early complications of high-dose methylprednisolone in acute spinal cord injury patients.* Injury, 2008. **39**(7): p. 748-752.
22. Alexander, J.K. and P.G. Popovich, *Neuroinflammation in spinal cord injury: therapeutic targets for neuroprotection and regeneration.* Progress in Brain Research, 2009. **175**: p. 125-137.
23. Popovich, P.G., et al., *Depletion of hematogenous macrophages promotes partial hindlimb recovery and neuroanatomical repair after experimental spinal cord injury.* Experimental Neurology, 1999. **158**(2): p. 351-365.
24. Giulian, D. and C. Robertson, *Inhibition of mononuclear phagocytes reduces ischemic injury in the spinal cord.* Annals of Neurology, 1990. **27**(1): p. 33-42.
25. Rapalino, O., et al., *Implantation of stimulated homologous macrophages results in partial recovery of paraplegic rats.* Nature Medicine, 1998. **4**(7): p. 814-821.
26. Frazen, R., et al., *Effects of macrophage transplantation in the injured adult rat spinal cord: A combined immunocytochemical and biochemical study.* Journal of Neuroscience Research, 1998. **51**(3): p. 316-327.
27. Prewitt, C.M., et al., *Activated macrophage/ microglial cells can promote the regeneration of sensory axons into the injured spinal cord.* Experimental Neurology, 1997. **148**(2): p. 433-443.
28. Bethea, J.R., *Spinal cord injury-induced inflammation: A dual-edged sword.* Progress in Brain Research, 2000. **128**: p. 33-43.
29. Zhang, B., et al., *Age decreases macrophage IL-10 expression: Implications for functional recovery and tissue repair in spinal cord injury.* Experimental Neurology, 2015. **273**: p. 83-91.
30. Lopes, R.L., et al., *IL-10 is required for polarization of macrophages to M2-like phenotype by mycobacterial DnaK (heat shock protein 70).* Cytokine, 2016. **85**: p. 123-129.
31. Thompson, C.D., et al., *The therapeutic role of interleukin-10 after spinal cord injury.* Journal of Neurotrauma, 2013. **30**(15): p. 1311-1324.
32. Zhou, Z., et al., *Interleukin-10 provides direct trophic support to neurons.* Journal of Neurochemistry, 2009. **110**(5): p. 1617-1627.
33. Genovese, T., et al., *Absence of endogenous interleukin-10 enhances secondary inflammatory process after spinal cord compression injury in mice.* Journal of Neurochemistry, 2009. **108**(6): p. 1360-1372.
34. Tuinstra, H.M., et al., *Multifunctional, multichannel bridges that deliver neurotrophin encoding lentivirus for regeneration following spinal cord injury.* Biomaterials, 2012. **33**(5): p. 1618-1626.

35. Boehler, R.M., et al., *Lentivirus delivery of IL-10 to promote and sustain macrophage polarization towards an anti-inflammatory phenotype.* Biotechnology and Bioengineering, 2014. **111**(6): p. 1210-1221.
36. Park, J., et al., *Reducing inflammation through delivery of lentivirus encoding for anti-inflammatory cytokines attenuates neuropathic pain after spinal cord injury.* Journal of Controlled Release, 2018. **290**: p. 88-101.
37. Park, J., et al., *Local Immunomodulation with Anti-inflammatory Cytokine-Encoding Lentivirus Enhances Functional Recovery after Spinal Cord Injury.* Molecular Therapy, 2018. **26**(7): p. 1756-1770.
38. Medicine, U.S.N.L.o., *Cells of the Nervous System.*
39. Spinal Cord Anatomy Lab, C.o.V.M., University of Minnesota, *Spinal Cord Anatomy: Spinal Cord White Matter.* 2013.
40. Gu, Z., et al., *Control of species-dependent cortico-motorneuronal connections underlying manual dexterity.* Science, 2017. **357**(6349): p. 400-404.
41. Yang, H.-W. and R. Lemon, *An electron microscopic examination of the corticospinal projection to the cervical spinal cord in the rat: lack of evidence for cortico-motoneuronal synapses.* Experimental Brain Research, 2003. **149**(4): p. 458-469.
42. Alstermark, B., J. Ogawa, and T. Isa, *Lack of monosynaptic corticomotoneuronal EPSPs in rats: disynaptic EPSPs mediated via reticulospinal neurons and polysynaptic EPSPs via segmental interneurons.* Journal of Neurophysiology, 2004. **91**(4): p. 1832-1839.
43. Canty, A. and M. Murphy, *Molecular mechanisms of axon guidance in the developing corticospinal tract.* Progress in Neurobiology, 2008. **85**(2): p. 214-235.
44. Maier, I.C. and M.E. Schwab, *Sprouting, regeneration and circuit formation in the injured spinal cord: factors and activity.* Philosophical Transactions of the Royal Society B: Biological Sciences, 2006. **361**(1473): p. 1611–1634.
45. Tetzlaff, W., et al., *Response of rubrospinal and corticospinal neurons to injury and neurotrophins.* Progress in Brain Research, 1994. **103**: p. 271-286.
46. Caroni, P., *Intrinsic neuronal determinants that promote axonal sprouting and elongation.* Bioessays, 1997. **19**(9): p. 767-775.
47. Bomze, H.M., et al., *Spinal axon regeneration evoked by replacing two growth cone proteins in adult neurons.* Nature Neuroscience, 2001. **4**(1): p. 38-43.
48. Lacroix, S. and M.H. Tuszynski, *Neurotrophic factors and gene therapy in spinal cord injury.* Neurorehabilitation and Neural Repair, 2000. **14**(4): p. 265-275.
49. Fawcett, J.W. and R.A. Asher, *The glial scar and central nervous system repair.* Brain Research Bulletin, 1999. **49**(6): p. 377-391.
50. Thomas, A.M., et al., *Channel density and porosity of degradable bridging scaffolds on axon growth after spinal injury.* Biomaterials, 2013. **34**(9): p. 2213-2220.
51. Schwab, M.E., *Repairing the injured spinal cord.* Science, 2002. **295**(5557): p. 1029-1031.
52. Cholas, R.H., H.-P. Hsu, and M. Spector, *The reparative response to cross-linked collagen-based scaffolds in a rat spinal cord gap model.* Biomaterials, 2012. **33**(7): p. 2050-2059.
53. Cholas, R.H., H.-P. Hsu, and M. Spector, *Collagen scaffolds incorporating select therapeutic agents to facilitate a reparative response in a standardized hemiresection defect in the rat spinal cord.* Tissue Engineering Part A, 2012. **18**(19-20): p. 2158-2172.

54. Yoshii, S., et al., *Bridging a spinal cord defect using collagen filament.* Spine, 2003. **28**(20): p. 2346-2351.
55. Cheng, H., et al., *Laminin-incorporated nerve conduits made by plasma treatment for repairing spinal cord injury.* Biochemical and Biophysical Research Communications, 2007. **357**(4): p. 938-944.
56. Menezes, K., et al., *Polylaminin, a polymeric form of laminin, promotes regeneration after spinal cord injury.* Federation of American Societies for Experimental Biology Journal, 2010. **24**(11): p. 4513-4522.
57. Zhang, Q., et al., *Multichannel silk protein/laminin grafts for spinal cord injury repair.* Journal of Biomedical Materials Research Part A, 2016. **104**(12): p. 3045-3057.
58. King, V., et al., *The use of injectable forms of fibrin and fibronectin to support axonal ingrowth after spinal cord injury.* Biomaterials, 2010. **31**(15): p. 4447-4456.
59. Lewandowski, G. and O. Steward, *AAVshRNA-mediated suppression of PTEN in adult rats in combination with salmon fibrin administration enables regenerative growth of corticospinal axons and enhances recovery of voluntary motor function after cervical spinal cord injury.* Journal of Neuroscience, 2014. **34**(30): p. 9951-9962.
60. Brazda, N., et al., *Experimental strategies to bridge large tissue gaps in the injured spinal cord after acute and chronic lesion.* Journal of Visualized Experiments, 2016. **2016**(111): p. e53331.
61. Koffler, J., et al., *Biomimetic 3D-printed scaffolds for spinal cord injury repair.* Nature Medicine, 2019. **25**(2): p. 263-269.
62. Dumont, C.M., et al., *Aligned hydrogel tubes guide regeneration following spinal cord injury.* Acta Biomaterialia, 2019. **86**: p. 312-322.
63. Hejčl, A., et al., *Dynamics of tissue ingrowth in SIKVAV-modified highly superporous PHEMA scaffolds with oriented pores after bridging a spinal cord transection.* Journal of Materials Science: Materials in Medicine, 2018. **29**(7): p. 89.
64. Pertici, V., et al., *Repair of the injured spinal cord by implantation of a synthetic degradable block copolymer in rat.* Biomaterials, 2014. **35**(24): p. 6248-6258.
65. Zamani, F., et al., *Promotion of spinal cord axon regeneration by 3D nanofibrous core-sheath scaffolds.* Journal of Biomedical Materials Research Part A, 2014. **102**(2): p. 506-513.
66. Moore, M.J., et al., *Multiple-channel scaffolds to promote spinal cord axon regeneration.* Biomaterials, 2006. **27**(3): p. 419-429.
67. Katoh, H., K. Yokota, and M.G. Fehlings, *Regeneration of Spinal Cord Connectivity Through Stem Cell Transplantation and Biomaterial Scaffolds.* Frontiers in Cellular Neuroscience, 2019. **13**: p. 248.
68. Assunção-Silva, R., et al., *Hydrogels and Cell Based Therapies in Spinal Cord Injury Regeneration.* Stem Cells International, 2015. **2015**: p. 948040.
69. Dumont, C.M., et al., *Spinal progenitor-laden bridges support earlier axon regeneration following spinal cord injury.* Tissue Engineering Part A, 2018. **24**: p. 1588-1602.
70. Keirstead, H.S. and W. Blakemore, *The role of oligodendrocytes and oligodendrocyte progenitors in CNS remyelination.* Advances in Experimental Medicine and Biology, 1999. **468**: p. 183-197.
71. Sharp, J. and H.S. Keirstead, *Therapeutic applications of oligodendrocyte precursors derived from human embryonic stem cells.* Current Opinion in Biotechnology, 2007. **18**(5): p. 434-440.

72. Cummings, B.J., et al., *Human neural stem cells differentiate and promote locomotor recovery in spinal cord-injured mice.* Proceedings of the National Academy of Sciences of the United States of America, 2005. **102**(39): p. 14069-14074.
73. Suzuki, H., et al., *Neural stem cell mediated recovery is enhanced by Chondroitinase ABC pretreatment in chronic cervical spinal cord injury.* PLoS One, 2017. **12**(8): p. e0182339.
74. Yokota, K., et al., *Engrafted Neural Stem/Progenitor Cells Promote Functional Recovery through Synapse Reorganization with Spared Host Neurons after Spinal Cord Injury.* Stem Cell Reports, 2015. **5**(2): p. 264-277.
75. Liu, Y., et al., *Transplants of fibroblasts genetically modified to express BDNF promote regeneration of adult rat rubrospinal axons and recovery of forelimb function.* Journal of Neuroscience, 1999. **19**(11): p. 4370-4387.
76. Tuszynski, M.H., et al., *Fibroblasts genetically modified to produce nerve growth factor induce robust neuritic ingrowth after grafting to the spinal cord.* Experimental Neurology, 1994. **126**(1): p. 1-14.
77. Xu, X., et al., *Axonal regeneration into Schwann cell-seeded guidance channels grafted into transected adult rat spinal cord.* Journal of Comparative Neurology, 1995. **351**(1): p. 145-160.
78. Xu, X., et al., *Bridging Schwann cell transplants promote axonal regeneration from both the rostral and caudal stumps of transected adult rat spinal cord.* Journal of Neurocytology, 1997. **26**(1): p. 1-16.
79. Kitamura, K., et al., *Application of Hepatocyte Growth Factor for Acute Spinal Cord Injury: The Road from Basic Studies to Human Treatment.* International Journal of Molecular Sciences, 2019. **20**(5): p. 1054.
80. Zhou, Y., et al., *Fibroblast growth factors in the management of spinal cord injury.* Journal of Cellular and Molecular Medicine, 2018. **22**(1): p. 25-37.
81. Ruitenberg, M.J., et al., *Ex vivo adenoviral vector-mediated neurotrophin gene transfer to olfactory ensheathing glia: effects on rubrospinal tract regeneration, lesion size, and functional recovery after implantation in the injured rat spinal cord.* Journal of Neuroscience, 2003. **23**(18): p. 7045-7058.
82. Facchiano, F., et al., *Promotion of regeneration of corticospinal tract axons in rats with recombinant vascular endothelial growth factor alone and combined with adenovirus coding for this factor.* Journal of Neurosurgery, 2002. **97**(1): p. 161-168.
83. Zhang, Y., et al., *NT-3 delivered by an adenoviral vector induces injured dorsal root axons to regenerate into the spinal cord of adult rats.* Journal of Neuroscience Research, 1998. **54**(4): p. 554-562.
84. Zhou, Z., et al., *HSV-mediated transfer of artemin overcomes myelin inhibition to improve outcome after spinal cord injury.* Molecular Therapy, 2009. **17**(7): p. 1173-1179.
85. Zhou, Z., et al., *IL-10 promotes neuronal survival following spinal cord injury.* Experimental Neurology, 2009. **220**(1): p. 183-190.
86. Liang, J., G. Deng, and H. Huang, *The activation of BDNF reduced inflammation in a spinal cord injury model by TrkB/p38 MAPK signaling.* Experimental and Therapeutic Medicine, 2018. **17**(3): p. 1688-1696.
87. Liu, S., et al., *Regulated viral BDNF delivery in combination with Schwann cells promotes axonal regeneration through capillary alginate hydrogels after spinal cord injury.* Acta Biomaterialia, 2017. **60**: p. 167-180.

88. Hassannejad, Z., et al., *Biofunctionalized peptide-based hydrogel as an injectable scaffold for BDNF delivery can improve regeneration after spinal cord injury.* Injury, 2019. **50**(2): p. 278-285.
89. Song, Z., et al., *Noninvasive, targeted gene therapy for acute spinal cord injury using LIFU-mediated BDNF-loaded cationic nanobubble destruction.* Biochemical and Biophysical Research Communications, 2018. **496**(3): p. 911-920.
90. Hernandez-Torres, V., et al., *BDNF effects on functional recovery across motor behaviors after cervical spinal cord injury.* Journal of Neurophysiology, 2017. **117**(2): p. 537-544.
91. Ghosh, B., et al., *Local BDNF delivery to the injured cervical spinal cord using an engineered hydrogel enhances diaphragmatic respiratory function.* Journal of Neuroscience, 2018. **38**(26): p. 5982-5995.
92. He, Z., et al., *An anti-inflammatory peptide and brain-derived neurotrophic factor-modified hyaluronan-methylcellulose hydrogel promotes nerve regeneration in rats with spinal cord injury.* International Journal of Nanomedicine, 2019. **14**: p. 721-732.
93. Butenschön, J., et al., *PSA-NCAM positive neural progenitors stably expressing BDNF promote functional recovery in a mouse model of spinal cord injury.* Stem Cell Resarch & Therapy, 2016. **7**(11).
94. Liang, W., et al., *The promotion of neurological recovery in the rat spinal cord crushed injury model by collagen-binding BDNF.* Biomaterials, 2010. **31**(33): p. 8634-8641.
95. Jain, A., et al., *In situ gelling hydrogels for conformal repair of spinal cord defects, and local delivery of BDNF after spinal cord injury.* Biomaterials, 2006. **27**(3): p. 497-504.
96. Uchida, S., et al., *Treatment of spinal cord injury by an advanced cell transplantation technology using brain-derived neurotrophic factor-transfected mesenchymal stem cell spheroids.* Biomaterials, 2016. **109**: p. 1-11.
97. Gransee, H., et al., *Localized delivery of brain-derived neurotrophic factor-expressing mesenchymal stem cells enhances functional recovery following cervical spinal cord injury.* Journal of Neurotrauma, 2015. **32**(3): p. 185-193.
98. Ji, X., et al., *Local injection of lenti-BDNF at the lesion site promotes M2 macrophage polarization and inhibits inflammatory response after spinal cord injury in mice.* Cellular and Molecular Neurobiology, 2015. **35**(6): p. 881-890.
99. Nakajima, H., et al., *Rescue of rat anterior horn neurons after spinal cord injury by retrograde transfection of adenovirus vector carrying brain-derived neurotrophic factor gene.* Journal of Neurotrauma, 2007. **24**(4): p. 703-712.
100. Nakajima, H., et al., *Targeted retrograde gene delivery of brain-derived neurotrophic factor suppresses apoptosis of neurons and oligodendroglia after spinal cord injury in rats.* Spine, 2010. **35**(5): p. 497-504.
101. Ziemlińska, E., et al., *Overexpression of BDNF increases excitability of the lumbar spinal network and leads to robust early locomotor recovery in completely spinalized rats.* PLoS One, 2014. **9**(2): p. e88833.
102. Han, Q., et al., *Linear ordered collagen scaffolds loaded with collagen-binding brain-derived neurotrophic factor improve the recovery of spinal cord injury in rats.* Tissue Engineering Part A, 2009. **15**(10): p. 2927-2935.
103. Zhao, T., et al., *Effects of retrograde gene transfer of brain-derived neurotrophic factor in the rostral spinal cord of a compression model in rat.* Molecular Biology Reports, 2012. **39**(8): p. 8045-8051.

104. Pawar, K., et al., *Biomaterial bridges enable regeneration and re-entry of corticospinal tract axons into the caudal spinal cord after SCI: association with recovery of forelimb function.* Biomaterials, 2015. **65**: p. 1-12.
105. De Laporte, L., et al., *Plasmid releasing multiple channel bridges for transgene expression after spinal cord injury.* Molecular Therapy, 2009. **17**(2): p. 318-326.
106. Smith, D.R., et al., *Combinatorial lentiviral gene delivery of pro-oligodendrogenic factors for improving myelination of regenerating axons after spinal cord injury.* Biotechnology and Bioengineering, 2019. **116**(1): p. 155-167.
107. Nishimune, H. and K. Shigemoto, *Practical anatomy of the neuromuscular junction in health and disease.* Neurologic Clinics, 2018. **36**(2): p. 231-240.
108. Tosolini, A.P., R. Mohan, and R. Morris, *Targeting the Full Length of the Motor End Plate Regions in the Mouse Forelimb Increases the Uptake of Fluoro-Gold into Corresponding Spinal Cord Motor Neurons.* Frontiers in Neurology, 2013. **4**.
109. Wu, P., et al., *Key changes in denervated muscles and their impact on regeneration and reinnervation.* Neural Regeneration Research, 2014. **9**(20): p. 1796-1809.
110. Kuffler, D.P., *Regeneration of muscle axons in the frog is directed by diffusible factors from denervated muscle and nerve tubes.* Journal of Comparative Neurology, 1989. **281**(3): p. 416-425.
111. Hepple, R.T. and C.L. Rice, *Innervation and neuromuscular control in ageing skeletal muscle.* Journal of Physiology, 2016. **594**(8): p. 1965-1978.
112. JW, G., et al., *Peripheral nerve repair and reconstruction.* Journal of Bone and Joint Surgery, 2013. **95**(23): p. 2144-2151.
113. Rowan, S.L., et al., *Denervation causes fiber atrophy and myosin heavy chain co-expression in senescent skeletal muscle.* PLoS One, 2012. **7**(1): p. e29082.
114. Spector, S.A., *Trophic effects on the contractile and histochemical properties of rat soleus muscle.* Journal of Neuroscience, 1985. **5**(8): p. 2189-2196.
115. Carlson, B.M., L. Billington, and J. Fauklner, *Studies on the regenerative recovery of long-term denervated muscle in rats.* Restorative Neurology and Neuroscience, 1996. **10**(2): p. 77-84.
116. Kalliainen, L.K., et al., *A specific force deficit exists in skeletal muscle after partial denervation.* Muscle & Nerve, 2002. **25**(1): p. 31-38.
117. Dow, D.E., et al., *Number of contractions to maintain mass and force of a denervated rat muscle.* Muscle & Nerve, 2004. **30**(1): p. 77-86.
118. Castro, M.J., et al., *Influence of complete spinal cord injury on skeletal muscle within 6 mo of injury.* Journal of Applied Physiology, 1999. **86**(1): p. 350-358.
119. Lotta, S., et al., *Morphometric and neurophysiological analysis of skeletal muscle in paraplegic patients with traumatic cord lesion.* Paraplegia, 1991. **29**(4): p. 247-252.
120. Round, J.M., et al., *Fiber areas and histochemical fiber types in the quadriceps muscle of paraplegic subjects.* Journal of the Neurological Sciences, 1993. **116**(2): p. 207-211.
121. Scelsi, R., et al., *Muscle fiber type morphology and distribution in paraplegic patients with traumatic cord lesion.* Acta Neuropathologica, 1982. **57**(4): p. 243-248.
122. Viguie, C.A., et al., *Quantitative study of the effects of long-term denervation on the extensor digitorum longus muscle of the rat.* Anatomical Record, 1997. **248**(3): p. 346-354.
123. Dumitru, A., et al., *Muscle changes during atrophy.* Advances in Experimental Medicine and Biology, 2018. **1088**: p. 73-92.

124. Niederle, B. and R. Mayr, *Course of denervation atrophy in type I and type II fibres of rat extensor digitorum longus muscle.* Anatomy and Embryology, 1978. **153**(1): p. 9-21.
125. Kraft, G.H., *Fibrillation potential amplitude and muscle atrophy following peripheral nerve injury.* Muscle & Nerve, 1990. **13**(9): p. 814-821.
126. Zealear, D.L., A.-L. Hamdan, and C.L. Ratney, *Effects of denervation on posterior cricoarytenoid muscle physiology and histochemistry.* Annals of Otology, Rhinology & Laryngology, 1994. **103**(10): p. 780-788.
127. Lu, D.-X., S.-K. Huang, and B.M. Carlson, *Electron microscopic study of long-term denervated rat skeletal muscle.* Anatomical Record, 1997. **248**(3): p. 355-365.
128. Prakash, Y., et al., *Inactivity-induced remodeling of neuromuscular junctions in rat diaphragmatic muscle.* Muscle & Nerve, 1999. **22**(3): p. 307-319.
129. Jiang, G.-L., et al., *Fibrillation potential amplitude to quantitatively assess denervation muscle atrophy.* Neuromuscular Disorders, 2000. **10**(2): p. 85-91.
130. Kostrominova, T.Y., et al., *Comparison of gene expression of 2-mo denervated, 2-mo stimulated-denervated, and control rat skeletal muscles.* Physiological Genomics, 2005. **22**(2): p. 227-243.
131. Listrat, A., et al., *How muscle structure and composition influence meat and flesh quality.* The Scientific World Journal, 2016. **2016**: p. 3182746.
132. Mathewson, M.A., et al., *Anatomical, architectural, and biochemical diversity of the murine forelimb muscles.* Journal of Anatomy, 2012. **221**(5): p. 443-451.
133. Pette, D. and G. Vrbová, *Neural control of phenotypic expression in mammalian muscle fibers.* Muscle & Nerve, 1985. **8**(8): p. 676-689.
134. Windisch, A., et al., *Fast to slow transformation of denervated and electrically stimulated rat muscle.* Journal of Physiology, 1998. **510**(2): p. 623-632.
135. Biering-Sørensen, B., et al., *Muscle after spinal cord injury.* Muscle & Nerve, 2009. **40**(4): p. 499-519.
136. Burnham, R., et al., *Skeletal muscle fibre type transformation following spinal cord injury.* Spinal Cord, 1997. **35**(2): p. 86-91.
137. Barat, M., P. Dehail, and M. de Seze, *Fatigue after spinal cord injury.* Annales de readaptation et de medecine physique, 2006. **49**(6): p. 277-282.
138. Pelletier, C. and A. Hicks, *Muscle characteristics an fatigue properties after spinal cord injury.* Critical Reviews in Biomedical Engineering, 2009. **37**(1-2): p. 139-164.
139. Fu, J., et al., *Exercise training promotes functional recovery after spinal cord injury.* Neural Plasticity, 2016. **2016**: p. 4039580.
140. Han, Q., et al., *Enhanced neuroprotection and improved motor function in traumatized rat spinal cords by rAAV2-mediated glial-derived neurotrophic factor combined with early rehabilitation training.* Chinese Medical Journal, 2014. **127**(24): p. 4220-4225.
141. Tashiro, S., et al., *Functional recovery from neural stem/progenitor cell transplantation combined with treadmill training in mice with chronic spinal cord injury.* Scientific Reports, 2016. **6**: p. 30898.
142. Nicola, F., et al., *Human dental pulp stem cells transplantation combined with treadmill training in rats after traumatic spinal cord injury.* Brazilian Journal of Medical and Biological Research, 2016. **49**(9): p. e5319.
143. Kao, C., et al., *Exogenous administration of glial cell line-derived neurotrophic factor improves recovery after spinal cord injury.* Resuscitation, 2008. **77**(3): p. 395-400.

144. Nothias, J., et al., *Combined effects of neurotrophin secreting transplants, exercise, and serotonergic drug challenge improve function in spinal rats.* Neurorehabilitation and Neural Repair, 2005. **19**(4): p. 296-312.
145. Askari, S., et al., *Effect of functional electrical stimulation (FES) combined with robotically assisted treadmill training on the EMG profile.* Conference Proceedings IEEE Engineering in Medicine and Biology Society, 2011. **2011**: p. 3043-3046.
146. Petrosyan, H., et al., *Spinal electro-magnetic stimulation combined with transgene delivery of neurotrophin NT-3 and exercise: novel combination therapy for spinal contusion injury.* Journal of Neurophysiology, 2015. **114**(5): p. 2923-2940.
147. Chao, T., et al., *A system to integrate electrical stimulation with robotically controlled treadmill training to rehabilitate stepping after spinal cord injury.* IEEE Transactions on Neural Systems and Rehabilitation Engineering, 2012. **20**(5): p. 730-737.
148. Field-Fote, E., *Combined use of body weight support, functional electric stimulation, and treadmill training to improve walking ability in individuals with chronic incomplete spinal cord injury.* Archives of Physical Medicine and Rehabilitation, 2001. **82**(6): p. 818-824.
149. Jung, R., et al., *Neuromuscular stimulation therapy after incomplete spinal cord injury promotes recovery of interlimb coordination during locomotion.* Journal of Neural Engineering, 2009. **6**(5): p. 055010.
150. Panisset, M., M. Galea, and D. El-Ansary, *Does early exercise attenuate muscle atrophy or bone loss after spinal cord injury?* Spinal Cord, 2016. **54**(2): p. 84-92.
151. Zhang, C., et al., *Early electrical field stimulation prevents the loss of spinal cord anterior horn motoneurons and muscle atrophy following spinal cord injury.* Neural Regeneration Research, 2018. **13**(5): p. 869-876.
152. Hou, J., et al., *Effect of simultaneous combined treadmill training and magnetic stimulation on spasticity and gait impairments following cervical spinal cord injury (C-SCI).* Journal of Neurotrauma, 2020. **[Epub ahead of print]**.
153. Marques, M., et al., *Locomotor training promotes time-dependent functional recovery after experimental spinal cord contusion.* Neuroscience, 2018. **392**: p. 258-269.
154. Burns, A., et al., *Fibrillation potentials following spinal cord injury: improvement with neurotrophins and exercise.* Muscle & Nerve, 2007. **35**(5): p. 607-613.
155. Gordon, T. and J. Mao, *Muscle atrophy and procedures for training after spinal cord injury.* Physical Therapy, 1994. **74**(1): p. 50-60.
156. Liu, K., et al., *PTEN deletion enhances the regenerative ability of adult corticospinal neurons.* Nature Neuroscience, 2010. **13**(9): p. 1075-1081.
157. Harel, N.Y. and S.M. Strittmatter, *Can regenerating axons recapitulate developmental guidance during recovery from spinal cord injury?* Nature Reviews Neuroscience, 2008. **7**(8): p. 603-616.
158. David, S., R. López-Vales, and V.W. Yong, *Chapter 30 - Harmful and beneficial effects of inflammation after spinal cord injury: potential therapeutic implications.* Handbook of Clinical Neurology, 2012. **109**: p. 485-502.
159. Smith, D.R., et al., *Polycistronic delivery of IL-10 and NT-3 promotes oligodendrocyte myelination and functional recovery in a mouse spinal cord injury model.* Tissue Engineering Part A, 2020. **00**(00).

160. Brewer, K., J. Bethea, and R. Yezierski, *Neuroprotective effects of interleukin-10 following excitotoxic spinal cord injury.* Experimental Neurology, 1999. **159**(2): p. 484-493.
161. Takami, T., et al., *Methylprednisolone and interleukin-10 reduce gray matter damage in the contused fischer rat thoracic spinal cord but do not improve functional outcome.* Journal of Neurotrauma, 2002. **19**(5): p. 653-666.
162. Ishii, H., et al., *ifn-γ-dependent secretion of IL-10 from Th1 cells and microglia/macrophages contributes to functional recovery after spinal cord injury.* Cell Death & Disease, 2013. **4**(7): p. e710.
163. Hellenbrand, D.J., et al., *Sustained interleukin-10 delivery reduces inflammation and improves motor function after spinal cord injury.* Journal of Neuroinflammation, 2019. **16**(1): p. 93.
164. Oruckaptan, H., et al., *Systemic administration of interleukin-10 attenuates early ischemic response following spinal cord ischemia reperfusion injury in rats.* Journal of Surgical Research, 2009. **155**(2): p. 345-356.
165. Jackson, C., et al., *Enhanced functional recovery from spinal cord injury following intrathecal or intramuscular administration of poliovirus replicons encoding IL-10.* Virology, 2005. **336**(2): p. 173-183.
166. Bethea, J.R., et al., *Systemically administered interleukin-10 reduces tumor necrosis factor-alpha production and significantly improves functional recovery following traumatic spinal cord injury in rats.* Journal of Neurotrauma, 1999. **16**(10): p. 851-863.
167. Koushki, D., et al., *Efficacy of some non-conventional herbal medications (sulforaphane, tanshinone IIA, and tetramethylpyrazine) in inducing neuroprotection in comparison with interleukin-10 after spinal cord injury: a meta-analysis.* Journal of Spinal Cord Medicine, 2015. **38**(1): p. 13-22.
168. Mapplebeck, J., S. Beggs, and M. Salter, *Sex differences in pain: a tale of two immune cells.* Pain, 2016. **157**: p. S2-6.
169. Rosen, S., B. Ham, and J. Mogil, *Sex differences in neuroimmunity and pain.* Journal of Neuroscience Research, 2017. **95**: p. 500-508.
170. Elkabes, S. and A.B. Nicot, *Sex steroids and neuroprotection in spinal cord injury: A review of preclinical investigations.* Experimental Neurology, 2014. **259**: p. 28-37.
171. Margul, D.J., et al., *Reducing neuroinflammation by delivery of IL-10 encoding lentivirus from multiple-channel bridges.* Bioengineering & Translational Medicine, 2016. **1**(2): p. 136-148.
172. Cummings, B.J., C. Engesser-Cesar, and A.J. Anderson, *Adaptation of a ladder beam walking task to assess locomotor recovery in mice following spinal cord injury.* Behavioural Brain Research, 2008. **117**(2): p. 232-241.
173. Schindelin, J., et al., *Fiji: an open-source platform for biological-image analysis.* Nature Methods, 2012. **9**(7): p. 676-682.
174. Wu, L., W. Cheng, and C. Shen, *Targeted depletion of TDP-43 expression in the spinal cord motor neurons leads to the development of amyotrophic lateral sclerosis-like phenotypes in mice.* Journal of Biological Chemistry, 2012. **287**(33): p. 27335-27344.
175. Labovitz, S., N. Robbins, and M. Fahim, *Endplate topography of denervated and disused rat neuromuscular junctions: comparison by scanning and light microscopy.* Neuroscience, 1984. **11**(4): p. 963-971.
176. Foundation, C.D.R., *Causes of a spinal cord injury.*

177. Kerschensteiner, M., et al., *In vivo imaging of axonal degeneration and regeneration in the injured spinal cord.* Nature Medicine, 2005. **11**(5): p. 572-577.
178. Lingor, P., et al., *Axonal degeneration as a therapeutic target in the CNS.* Cell and Tissue Research, 2012. **349**(1): p. 289-311.
179. Hassannejad, Z., et al., *The fate of neurons after traumatic spinal cord injury in rats: A systematic review.* Iranian Journal of Basic Medical Sciences, 2018. **21**(6): p. 546-557.
180. Yong, C., et al., *Apoptosis in cellular compartments of rat spinal cord after severe contusion injury.* Journal of Neurotrauma, 1998. **15**(7): p. 459-472.
181. Apel, P.J., et al., *How age impairs the response of the neuromuscular junction to nerve transection and repair.* Journal of Orthopaedic Research, 2009. **27**(3): p. 385-393.
182. Wilson, M. and M. Deschenes, *The neuromuscular junction: anatomical features and adaptations to various forms of increased, or decreased neuromuscular activity.* International Journal of Neuroscience, 2005. **115**(6): p. 803-828.
183. Farooque, M., et al., *Gender-related differences in recovery of locomotor function after spinal cord injury in mice.* Spinal Cord, 2006. **44**: p. 182-187.
184. Hauben, E., et al., *Sexual dimorphism in the spontaneous recovery from spinal cord injury: a gender gap in beneficial autoimmunity?* European Journal of Neuroscience, 2002. **16**(9): p. 1731-1740.
185. Deitch, E.A., et al., *Neutrophil activation is modulated by sex hormones after trauma-hemorrhagic shock and burn injuries.* American Journal of Physiology: Heart and Circulatory Physiology, 2006. **291**(3): p. H1456-H1465.
186. Thomas, C.K. and I. Zijdewind, *Fatigue of muscles weakened by death of motoneurons.* Muscle & Nerve, 2005. **33**(1): p. 21-41.
187. Cregg, J.M., et al., *Functional regeneration beyond the glial scar.* Experimental Neurology, 2014. **253**: p. 197-207.
188. Tuinstra, H.M., et al., *Long-term characterization of axon regeneration and matrix changes using multiple channel bridges for spinal cord regeneration.* Tissue Engineering Part A, 2014. **20**(5-6): p. 1027-1037.
189. Breen, B.A., et al., *Therapeutic effect of neurotrophin-3 treatment in an injectable collagen scaffold following rat spinal cord hemisection injury.* ACS Biomaterials Science & Engineering, 2017. **3**(7): p. 1287-1295.
190. Chedly, J., et al., *Physical chitosan microhydrogels as scaffolds for spinal cord injury restoration and axon regeneration.* Biomaterials, 2017. **138**: p. 91-107.
191. Ando, K., et al., *Self-assembling peptide reduces glial scarring, attenuates posttraumatic inflammation, and promotes neurite outgrowth of spinal motor neurons.* Spine (Phila Pa 1976), 2016. **41**(20): p. E1201-E1207.
192. Liu, S., Y.-Y. Xie, and B. Wang, *Role and prospects of regenerative biomaterials in the repair of spinal cord injury.* Neural Regeneration Research, 2019. **14**(8): p. 1352-1363.
193. Tysseling-Mattiace, V.M., et al., *Self-assembling nanofibers inhibit glial scar formation and promote axon elongation after spinal cord injury.* Journal of Neuroscience, 2008. **28**(14): p. 3814-3823.
194. Khaing, Z.Z., et al., *High molecular weight hyaluronic acid limits astrocyte activation and scar formation after spinal cord injury.* Journal of Neural Engineering, 2011. **8**(4): p. 046033.

195. McCreedy, D.A., et al., *Semi-Automated Counting of Axon Regeneration in Poly(Lactide Co-Glycolide) Spinal Cord Bridges.* Journal of Neuroscience Methods, 2016. **263**: p. 15-22.
196. Lee, E., et al., *ACT-PRESTO: Rapid and consistent tissue clearing and labeling method for 3-dimensional (3D) imaging.* Scientific Reports, 2016. **6**(18631).
197. Yang, B., et al., *Single-Cell Phenotyping within Transparent Intact Tissue Through Whole-Body Clearing.* Cell, 2014. **158**(4): p. 945-958.
198. Pomeshchik, Y., et al., *Interleukin-33 treatment reduces secondary injury and improves functional recovery after contusion spinal cord injury.* Brain, Behavior, and Immunity, 2015. **44**: p. 68-81.
199. Samantaray, S., et al., *Neuroprotective efficacy of estrogen in experimental spinal cord injury in rats.* Annals of the New York Academy of Sciences, 2011. **1199**: p. 90-94.
200. Tedeschi, A., et al., *The calcium channel subunit alpha2delta2 suppresses axon regeneration in the adult CNS.* Neuron, 2016. **92**(2): p. 267-269.
201. Ding, C. and M. Hammarlund, *Aberrant information transfer interferes with functional axon regeneration.* Elife, 2018. **7**: p. e38829.
202. Dace, D., et al., *Interleukin-10 overexpression promotes fas-ligand-dependent chronic macrophage-mediated demyelinating polyneuropathy.* PLoS One, 2009. **4**(9): p. e7121.
203. Markusic, D., et al., *Comparison of single regulated lentiviral vectors with rtTA expression driven by an autoregulatory loop or a constitutive promoter.* Nucleic Acids Research, 2005. **33**(6): p. e63.
204. Toniatti, C., et al., *Gene therapy progress and prospects: Transcription regulatory systems.* Gene Therapy, 2004. **11**(8): p. 649-657.
205. Clackson, T., *Regulated gene expression systems.* Gene Therapy, 2000. **7**(2): p. 120-125.
206. al Yacoub, N., et al., *Optimized production and concentration of lentiviral vectors containing large inserts.* Journal of Gene Medicine, 2007. **9**(7): p. 579-584.